Localized Surface Plasmon Resonance in Bimetallic Core-Shell Nanoparticles

Supervisor:

Avijit Das

Submitted by:

Syeda Adiba Mirzana Rahman - 12121168
Ishmam Salim Chowdhury - 13121031
Simanta Siddha - 12121125
Md. Mahmudul Hasan - 12121135

Submitted to the Department of Electrical and Electronics Engineering, BRAC University

In partial fulfillment of the requirements for the degree of Bachelor of Science
December 2016

Declaration

We, hereby, declare that this thesis is based on self-derived results. Materials that support our work by other researchers are mentioned in the reference section. This Thesis, neither in whole or in part, has been previously submitted for any degree.

Signature of the Supervisor: **Signature of the authors:**

_____   _____
       Avijit Das   Ishmam Salim Chowdhury

_____
Md. Mahmudul Hasan

_____
Simanta Siddha

_____
Syeda Adiba Mirzana Rahman

Acknowledgement

Abstract

Colloidal nanoparticles have unique Localized Surface Plasmon Resonance (LSPR) properties. Various applications for LSPRs are in optics, photo catalysis, medicine and photovoltaics. For our research, we use the Mie Theory to analyze the LSPR properties of bimetallic core-shell nanoparticles in the shape of a sphere and consisting of Drude metals. We have come to see that there is a special LSPR mode in the interface between the two metals, i.e. the core and the shell, whose energy is concentrated at both the inner and the outer surfaces of the bimetallic nanoparticle. These phenomena are known as Ordinary Surface Plasmon Resonance and Extraordinary Surface Plasmon Resonance for the outer and inner surfaces respectively. The shape of the extinction spectrum and the shift of LSPR peak as a function of various geometric parameters are determined by both the Ordinary and Extraordinary LSPR modes together. When extended to practical noble metals such as Gold (Au) and Silver (Ag), we find that the SPR of Au@Ag (Gold core and Silver shell) nanoparticles can occur in the visible region with high tunability, which is beneficial to the enhancement of bio-sensing. Previous research has shown that Ordinary Plasmon Resonance can be used for bio-sensing by using one metal. In this paper, we will see that Extraordinary Plasmon Resonance can also be used to for bio-sensing. By changing the parameters of the core and the shell, and the substrate material, we will see the change in the Power Absorption curve, the electric field coupling, Sensitivity of the biomolecule and the SPR Shift.

Table of Contents

List of Figures

1. Introduction

Nanoparticles have unique properties and capabilities; which is why they have been quite interesting in a number of different fields for many years. A few of these properties are a glimpse of hope in the developing field of solar technology, where efficiency low costs are dominant factors in creating new technologies. Localized Surface Plasmon Resonance (LSPR) in bimetallic core shell nanoparticles has also been a topic of interest for many researchers over the years.

1.1 Nanoplasmonics

In the year 1957, Rufus Ritchie was the first person to predict the existence of surface plasmons. Surface plasmons were thoroughly studied by many scientists for the next 20 years. T. Turbadar studied in the 1950s and 1960s, and Heinz Raether, E. Kretschmann, and A. Ottio in the 1960s and 1970s. **Plasmonics** is the transfer of information in nanoscale structures by means of plamons.

Light scattering of minute nanoparticles is a fascinating research interest for a range of applications. It starts from the energy sector, where they are used to escalate the efficiency of solar cells, and goes all the way to the medical sector, where they are used to they play a part in the imagery and drug delivery systems. The mode by which these nanoparticles scatter light is extremely crucial to the research. Light scattering is the reduction or weakening of a beam of light by particles, either by absorption or by scattering. The summation of these two parts is known as the **extinction** [2].

Nanoplasmonics is the study of optical phenomena in the nanoscale vicinity of metal surfaces [4]. Due to the excitation of localized surface plasmons, noble-metal nanoparticles that are of size smaller than the wavelength of light in the visible region, show strong resonances for light scattering and absorption. At the point of resonance, light resonantly energizes and causes combined oscillation of the conduction electrons of the metal nanoparticle, which in turn acts as a regular dipole. Its resonance frequency is strongly dependent on the shape of the particle and the dielectric environment (which we will try to show in our thesis paper). This phenomenon enables us to tune its color throughout the visible region and into the near-infrared (IR) regime of the electromagnetic spectrum, while keeping the size of the particle a lot below the 100 nm range [5].

One of the most protruding applications of this phenomenon has played a part in history, i.e. in the form of colored glass with regards to metal nanoparticle dopants. A dopant, otherwise known as a doping agent, is a trace impurity element that is inserted into a substance in very low

concentrations to alter the electrical or optical properties of the substance. More modern applications that deal with a single nanoparticle involve the tagging of biomolecules, improvement of light emission from nanoscale photon sources, and biomolecular sensing. All of these properties exploit the fact that metal nanoparticles enable nano-concentration of light below the diffraction limit around the particle surface at their dipolar resonant frequencies, and feature resonantly enhanced absorption and scattering cross-sections [5].

Some of the equipment of the **London Centre for Nanotechnology** (LCN) is fundamental for the study and fabrication of the structures needed in nanoplasmonics; high resolution **Transmission Electron Microscopy** (TEM) disentangles the properties of plasmonic modes in complex structures. **Electron Beam Lithography** or **Focused Ion Beam Milling** is necessary to produce metallic structures with properties in the visible range. In order to make sure that the samples to be investigated have the desired dimensions and morphology, high resolution **Scanning Electron Microscope** (SEM) imaging is required [5].
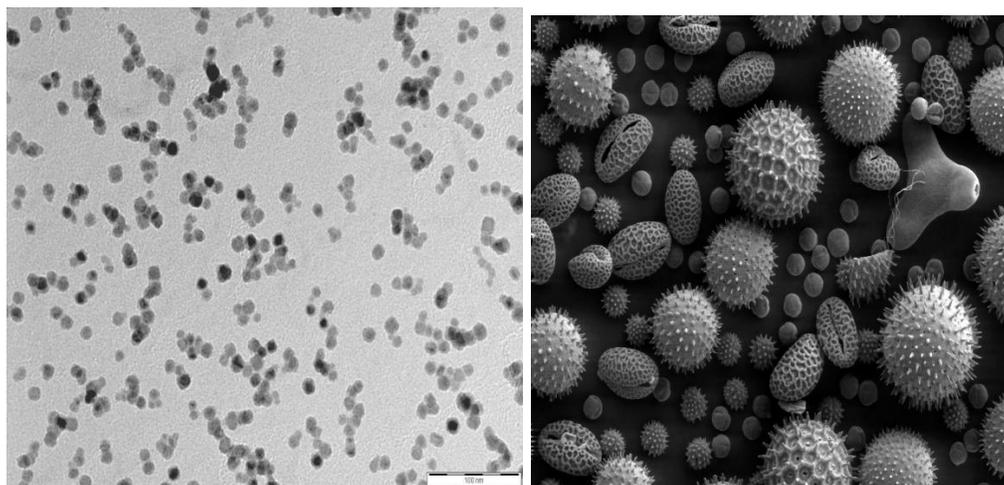
Figure 1.1 *(a) Images of Silver (Ag) nanoparticles obtained from Transmission Electron Microscopy (TEM),* [18], *(b) Images obtained from Scanning Electron Microscope (SEM),* [19]

1.2 Surface Plasmon Resonance in the Medical Sector

Since the plasmonic connection between metal nanoparticles is extremely sensitive to their partition and to the refractive list of the encompassing medium, surface plasmon resonance are utilized as a part of biological, chemical, and medical sensing and recognition applications. The resonance shift because of a changing dielectric environment may take into account the recognizable proof of various chemicals. In such cases, a thin metal layer or surface containing a thick or surface containing a thick measure of nanoparticles is organized. These metal nanoparticles can be made sensitive to unique sorts of biomolecules amid functionalization. At the point when the researched substance is spread over the surface, particular official of the species to the nanoparticles will bring about a huge move in Localized Surface Plasmon Resonance. Besides, functionalized nanoparticles can be infused into cells; they will tie with particular atoms and afterward can be found effectively and productively [6].

Plasmonic interaction between metal nanoparticles is very sensitive to their separation. As a result, precise measurements of the plasmon resonance wavelength of metal particle assemblies functionalized with biomolecules can be used as a molecular-scale ruler that operates over a length of scale much larger than that in the fluorescence energy transfer metrology that is regularly used in biology. Practical usage of this concept is adopted in systems biology, for example, imaging of the motion of molecular motors or of structural changes in proteins and in DNA [6].

Another example for a promising application is the use of particles composed of a dielectric core and a metallic shell in cancer treatment. When these particles are injected into the human body, they are selectively bound to malicious (harmful or mutated) cells. This is when laser sterilization at a precisely engineered plasmon resonance wavelength is used to heat the particles and finally destroy the cells [6].

1.3 Overview of the thesis

Chapter 1

This chapter gives us an introduction to Nanoplasmonics and talks about its various applications in optics, photovoltaics etc. and also in the medical sector.

Chapter 2

This part of the paper deals with Surface Plasmon Resonance (SPR) and Localized Surface Plasmon Resonance (LSPR), the physics behind LSPR and the advantages of LSPR over SPR.

Chapter 3

Here, we talked about our proposed structure and the biomolecules that are present in the human body and their functions.

Chapter 4

We have elaborated on the differentces between Ordinary Plasmon Resonance and Extraordinary Plasmon Resonance. It contains a brief introduction bout Lumerical: the software that we have used for our research. Moreover, it has a detailed outline about how we have used the software to create our desired experimental setup.

Chapter 5

Finally, this part is all about the simulation process, the research and the analysis. Graphs of Power Absorption, SPR Shift and Sensitivity of the biomolecule, and the Electric Field coupling are displayed along with the explanations.

Chapter 6

Lastly, this chapter is the conclusion to our thesis paper. We have talked about the fabrication of the nanoparticle as well. Moreover, we mentioned the limitations of our study.

2. Physics of LSPR

2.1 Surface Plasmon Resonance and Localized Surface Plasmon Resonance

Surface Plasmons (SP)

Surface plasmons are coherent delocalized electron oscillations that exist at the interface between any two materials where the real part of the dielectric constant changes sign across the interface (e.g. a metal-dielectric interface). There are evanescent waves on both sides of the interface
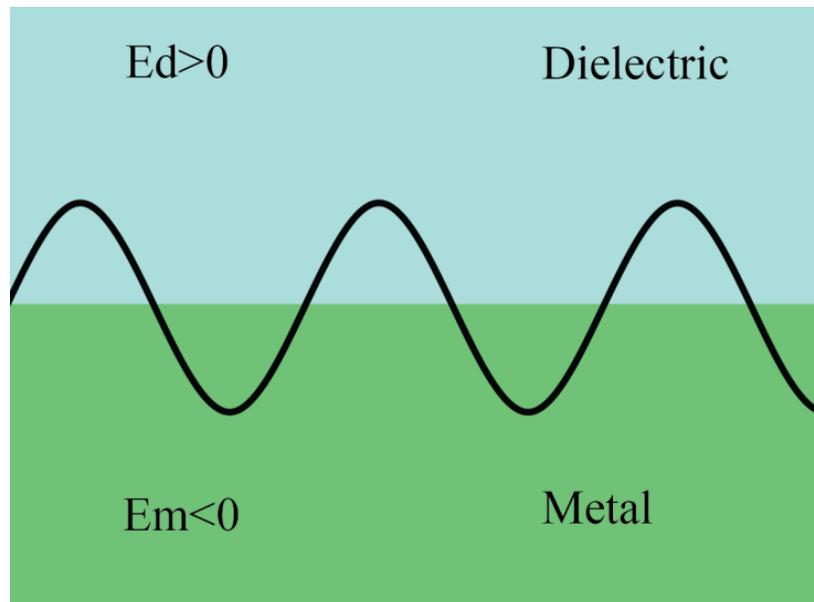
Figure 2.1 *Surface plasmon*

E_d = Permittivity of the dielectric
E_m = Permittivity of the metal

2.2 Evanescent Waves

An evanescent wave is a near field wave with an intensity that exhibits exponential decay without absorption as a function of distance from the boundary at which the wave was formed. This means that the energy is confined in a small area in that wave.

There is decay on both sides of the interface and the wave only propagates in the longitudinal direction.
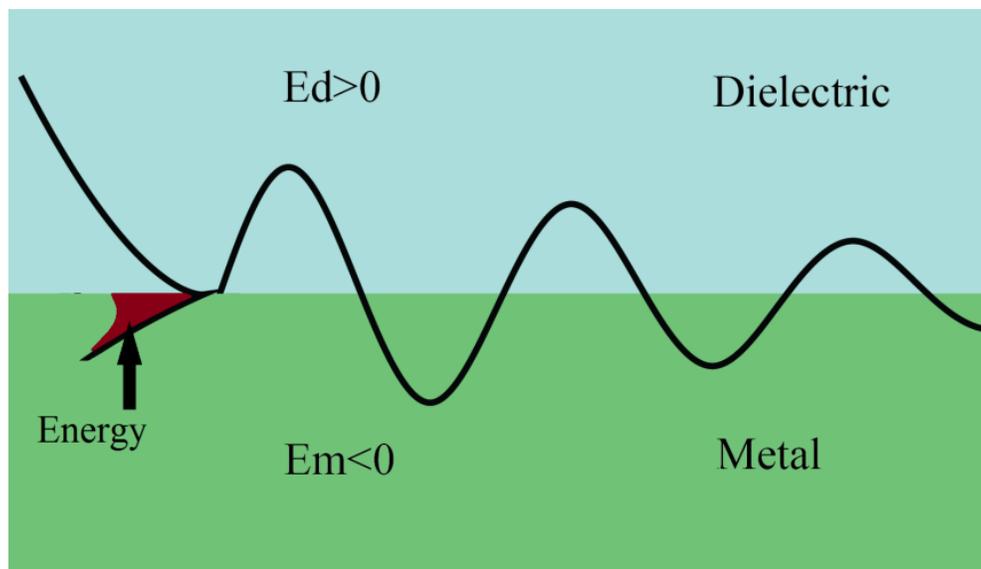
Figure 2.2 *Evanescent wave*

Surface plasmons have lower energy than bulk (or volume) plasmons which quantize the longitudinal electron oscillations about positive ion cores within the bulk of an electron cloud or plasma. The charge motion in an SP creates electromagnetic fields both inside and outside the metal. The total excitation, i.e. the charge motion and the associated electromagnetic field, is called a surface plasmon (or surface plasmon polariton, SPP) at a planar interface, or a localized surface plasmon for a small particle.

2.3 Surface Plasmon Resonance (SPR)

Surface plasmon resonance is the resonant oscillation of conduction electrons at the interface between negative (Em<0) and positive (Ed>0) permittivity material stimulated by incident light. When the frequency of the incident light is the same as the natural frequency of the surface electrons, the resonance condition is established, forcing the electrons to oscillate against the restoring force of the positive nuclei. Surface plasmon resonance in subwavelength scale nanostructures can be polaritonic or plamonic in nature [7].
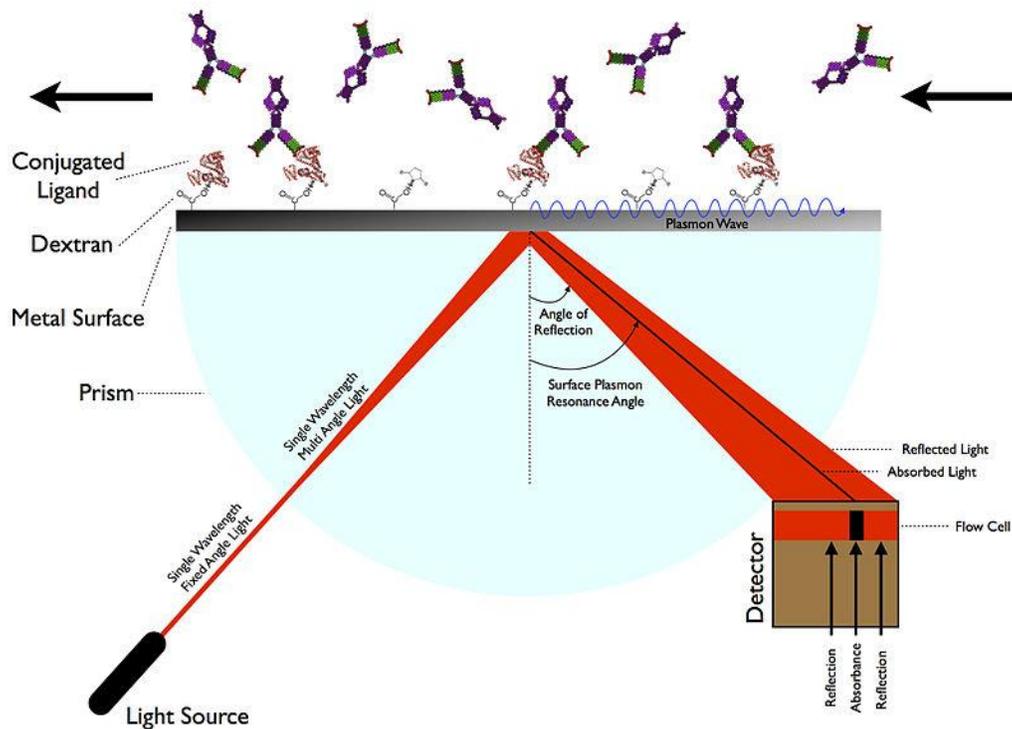
Figure 2.3 *Surface Plasmon Resonance* [7]

SPR is the excitation of a coupled state between photons and plasma oscillations at the interface between a metal and a dielectric [8].

- Radiative surface plasmons are coupled with propagating electromagnetic waves
- Non-radiative surface plasmons do not couple with propagating electromagnetic waves
- Surface plasmon polarizations (SPPs) are always non-radiative for perfectly flat surfaces

In contrary to conventional wave guides, field on both sides are always evanescent.
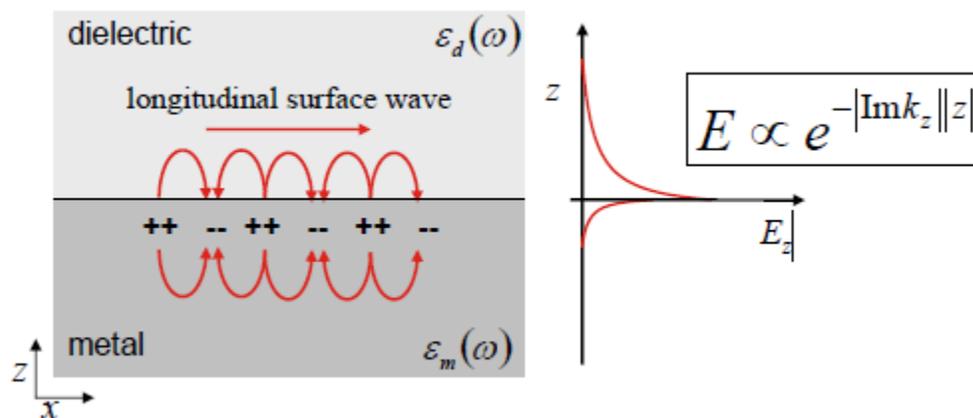
Figure 2.4 *Schematic of Surface Plasmon Resonance* [8]

2.4 Localized Surface Plasmon Resonance (LSPR)

This paper mainly concerns with Localized Surface Plasmon Resonance (LSPR).

A Localized Surface Plasmon (LSP) is the result of the confinement of a surface plasmon in a nanoparticle of size comparable or smaller than the wavelength of the light in the visible range or the light used to excite the plasmon. LSP has two important effects:

- Electric fields near the particle's surface are greatly enhanced. This enhancement falls off quickly if the distance from the surface is increased.
- The particle's optical absorption has a maximum at the plasmon resonant frequency. For noble metal nanoparticles, this occurs at visible wavelengths. For semiconductor nanoparticles, the maximum optical absorption occurs in the near-infrared or mid-infrared region.

Localized Surface Plasmons are **non-propagating** excitations of the conduction electrons of metallic nanostructures coupled to the electromagnetic field. These modes generate naturally from the scattering problem of a small, sub-wavelength conductive nanoparticle in an oscillating electromagnetic field. An operative restoring force is exerted on the driven electrons by the curved surface of the nanoparticle. As a result, a resonance arises, leading to field amplification on both inside and in the near-field zone outside the particle. This resonance is called **localized surface plasmon resonance**. Another significance of the curved surface is that the plasmon resonances can be generated by direct light illumination [5].

For gold and silver nanoparticles, the resonance falls into the visible range of the electromagnetic spectrum. It is solely because of this that the bright colors are displayed by particles both in

transmitted and reflected light, due to resonantly improved absorption and scattering. This application has made itself very useful for many centuries, for example, in the staining of glass in windows or ornamental cups [5].
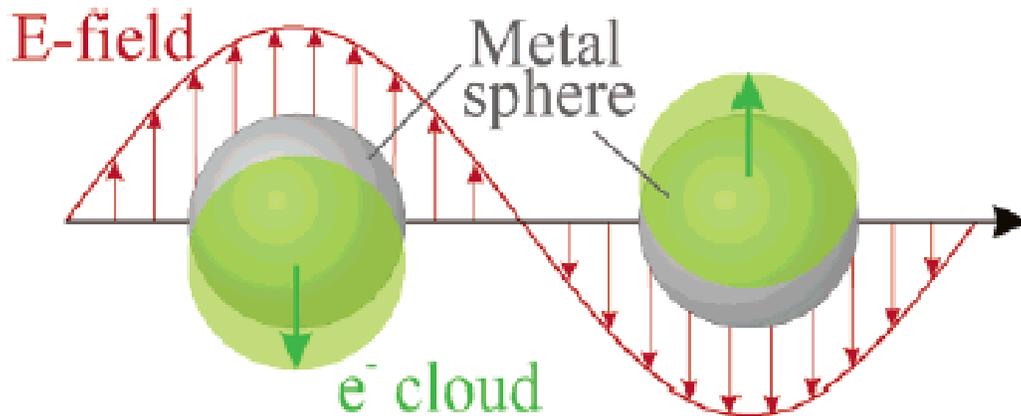
Figure 2.5 *Schematic of Localized Surface Plasmon oscillation of a sphere, showing the displacement of the conduction electron charge cloud relative to the nuclei.* [2]

2.5 LSPR in a Metal Sphere

The interaction of a particle of size *d* with the electromagnetic field can be analyzed by using the **Quasi-Static** approximation, given that $d<<\lambda$, that is, the particle is far smaller than the wavelength of the incident light surrounding the medium. In a case like this, the phase of the harmonically oscillating electromagnetic field is virtually constant over the particle volume. Hence, it is possible to calculate the spatial field distribution by assuming the simplified problem of a particle in an electrostatic field. Once the field distributions are acknowledged, the harmonic time dependence can then be added to the solution. This lowest-order estimation of the full scattering problem describes the optical properties of nanoparticles of proportions below 100 nm, effectively for many purposes [5].

We start with the simplest geometry for an analytical treatment: a homogeneous, isotropic sphere of radius *a*, positioned at the origin in a uniform, static electric field, $\mathbf{E} = E_0\ \hat{\mathbf{z}}$. the surrounding medium is isotropic and non-absorbing with dielectric constant ε_m, and the field lines are parallel to the z-direction at an adequate amount of distance from the sphere. The dielectric response of the sphere is further described by the dielectric function $\varepsilon\ (\omega)$, which we consider as a simple complex number ε for the time being [5].

Approaching from an electrostatic point of view, we are concerned in a solution of the **Laplace equation** for the potential, $\nabla_2\Phi = 0$, from which we will be able to calculate the electric field, $\mathbf{E} = -\nabla\Phi$. Due to the azimuthal symmetry of the problem, the general solution is of the form:

$$\Phi(r,\theta) = \sum_{l=0}^{\infty}\left[A_l r^l + B_l r^{-(l+1)}\right]P_l(\cos\theta),$$
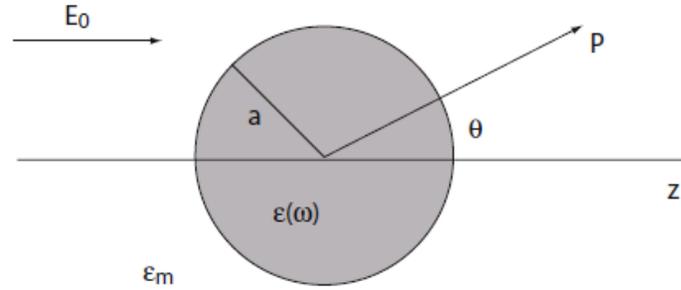
Figure 2.6 *Sketch of a homogeneous sphere in an electrostatic field* [5]

where $P_l(\cos\theta)$ are the Legendre Polynomials of order l, and θ the angle between the position vector $\mathbf{r}$, at point P and the z-axis. Due to the requirement that the potentials remain finite at the origin, the solution for the potentials Φ_{in} inside and Φ_{out} outside the sphere can be written as:

$$\Phi_{in}(r,\theta) = \sum_{l=0}^{\infty}A_l r^l P_l(\cos\theta)$$

$$\Phi_{out}(r,\theta) = \sum_{l=0}^{\infty}\left[B_l r^l + C_l r^{-(l+1)}\right]P_l(\cos\theta).$$

The coefficients A_l, B_l and C_l can now be determined form the boundary conditions at $r \to \infty$ and at the sphere surface $r = a$. The requirement that $\Phi_{in}\to -E_0 z = -E_0 r \cos\theta$ as $r \to \infty$ demands that $B_l = -E_0$ and $B_l = 0$ for $l \neq 1$. The remaining coefficients A_l and C_l are defined by the boundary conditions at $r = a$. equality of the tangential components of the electric field demands that

$$-\frac{1}{a}\frac{\partial\Phi_{in}}{\partial\theta}\bigg|_{r=a} = -\frac{1}{a}\frac{\partial\Phi_{out}}{\partial\theta}\bigg|_{r=a},$$

And the equality of the normal components of the displacement field

$$-\varepsilon_0\varepsilon\frac{\partial\Phi_{in}}{\partial r}\bigg|_{r=a} = -\varepsilon_0\varepsilon_m\frac{\partial\Phi_{out}}{\partial r}\bigg|_{r=a}.$$

Application of these boundary conditions leads to $A_l = C_l = 0$ for $l \neq 1$, and via the calculation of the remaining coefficients A_l and C_l, the potentials evaluate to:

$$\Phi_{in} = -\frac{3\varepsilon_m}{\varepsilon + 2\varepsilon_m} E_0 r \cos\theta$$

$$\Phi_{out} = -E_0 r \cos\theta + \frac{\varepsilon - \varepsilon_m}{\varepsilon + 2\varepsilon_m} E_0 a^3 \frac{\cos\theta}{r^2}.$$

It is interesting to interpret the w=equation physically: Φ_{out} describes the superposition for the applied field and that of a dipole located at the particle center. We can rewrite Φ_{out} by introducing the dipole moment **p** as:

$$\Phi_{out} = -E_0 r \cos\theta + \frac{\mathbf{p} \cdot \mathbf{r}}{4\pi\varepsilon_0\varepsilon_m r^3}$$

$$\mathbf{p} = 4\pi\varepsilon_0\varepsilon_m a^3 \frac{\varepsilon - \varepsilon_m}{\varepsilon + 2\varepsilon_m} \mathbf{E}_0.$$

Therefore, we see that the applied field introduces a dipole moment inside the sphere of magnitude proportional to $|\mathbf{E}_0|$. If we introduce the polarizability a:

$$\alpha = 4\pi a^3 \frac{\varepsilon - \varepsilon_m}{\varepsilon + 2\varepsilon_m}.$$

This equation is the central result of this section, the complex polarizability of a small sphere of sub-wavelength diameter in the electrostatic approximation. We note that it shows the same functional form as the Clausius-Mossotti relation.

The following figure (Fig. 2.7) shows the absolute value and phase of a with respect to frequency ω (in energy units) for a dielectric constant varying as $\varepsilon(\omega)$ of the Drude form, in this case fitted to the dielectric response of silver [Johnson and Christy, 1972]. It is obvious that the polarizability experiences a resonant improvement under the condition that $|\varepsilon + 2\varepsilon_m|$ is a minimum, which for the case of small or slowly varying $Im[\varepsilon]$ around the resonance simplifies to:

$$Re\left[\varepsilon(\omega)\right] = -2\varepsilon_m.$$

This relationship is called the Fröhlich condition and the associated mode (in an oscillating field) the *dipole surface plasmon* of the metal nanoparticle. For a sphere consisting of a Drude metal with a dielectric function located in air, the Fröhlich criterion is met at the frequency $\omega_0 = \omega_p/\sqrt{3}$, which further expresses the strong dependence of the resonance frequency on the dielectric environment: The resonance red shifts as ε_m is increased. Metal nanoparticles are thus the ideal platforms for optical sensing of change in refractive index.
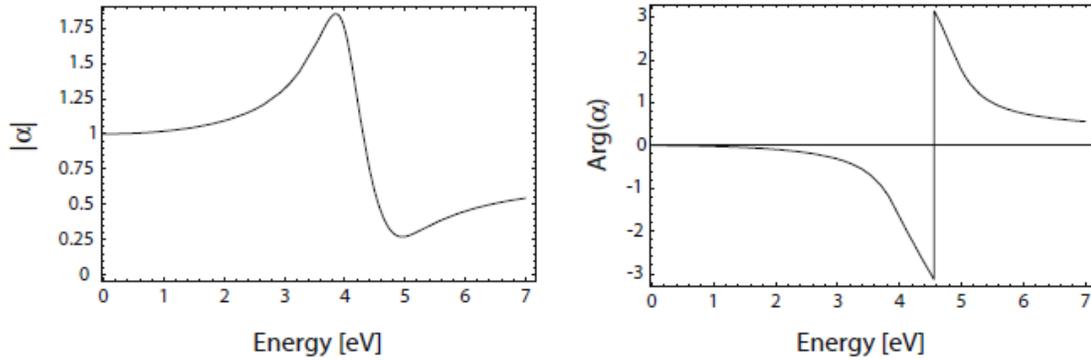
Figure 2.7 *Absolute value and field polarizability α of a sub-wavelength metal nanoparticle with respect to frequency of the driving field (expressed as eV units). Here, ε(ω) is taken as a Drude fit to the dielectric function of silver [Johnson and Christy. 1972].[5]*

We note that the magnitude of α at resonance is limited by the incomplete vanishing of its denominator, due to $\text{Im}[\varepsilon(\omega)] \neq 0$.

The distributions of the electric field $\mathbf{E} = -\nabla\Phi$ can be evaluated from the potentials to:

$$\mathbf{E_{in}} = \frac{3\varepsilon_m}{\varepsilon + 2\varepsilon_m}\mathbf{E_0}$$

$$\mathbf{E_{out}} = \mathbf{E_0} + \frac{3\mathbf{n}\,(\mathbf{n}\cdot\mathbf{p}) - \mathbf{p}}{4\pi\,\varepsilon_0\varepsilon_m}\frac{1}{r^3}.$$

The resonance in α also implies a resonant enhancement of both the internal and dipolar fields. It is this field enhancement at the plasmon resonance on which many of the prominent applications of metal nanoparticles in optical devices and sensors rely.

We have been on the firm ground of electrostatics, which we will now leave and turn our attention to the electromagnetic fields radiated by a small particle excited at its plasmon resonance. For a small sphere $a \ll \lambda$, its representation as an ideal dipole is valid in the Quasi-Static regime, i.e. it allows for time-varying fields but neglects spatial retardation effects over the particle volume. Under plane-wave illumination with $\mathbf{E}(\mathbf{r},\, t) = \mathbf{E_0}e^{-i\omega t}$, the fields introduce an oscillating dipole moment $\mathbf{p}(t) = \varepsilon_0\varepsilon_m\alpha\mathbf{E_0}e^{-i\omega t}$, with α given by the electrostatic result. The radiation of this dipole leads to *scattering* of the plane wave by the sphere, which can be represented as radiation by a point dipole.

It is useful to briefly review the basics of the electromagnetic fields associated with an oscillating electric dipole. The total fields $\mathbf{H}(t) = \mathbf{H}e^{-i\omega t}$ and $\mathbf{E}(t) = \mathbf{E}e^{-i\omega t}$ in the near immediate zones of a dipole can be written as:

$$\mathbf{H} = \frac{ck^2}{4\pi} (\mathbf{n} \times \mathbf{p}) \frac{e^{ikr}}{r} \left(1 - \frac{1}{ikr}\right)$$

$$\mathbf{E} = \frac{1}{4\pi\varepsilon_0\varepsilon_m} \left\{ k^2 (\mathbf{n} \times \mathbf{p}) \times \mathbf{n} \frac{e^{ikr}}{r} + [3\mathbf{n} (\mathbf{n} \cdot \mathbf{p}) - \mathbf{p}] \left(\frac{1}{r^3} - \frac{ik}{r^2}\right) e^{ikr} \right\},$$

With $k = 2\pi/\lambda$ and **n** the unit vector in the direction of the point P of interest. In the near zone *(kr << 1)*, the electrostatic result for the electric field is recovered,

$$\mathbf{E} = \frac{3\mathbf{n} (\mathbf{n} \cdot \mathbf{p}) - \mathbf{p}}{4\pi\varepsilon_0\varepsilon_m} \frac{1}{r^3}$$

And the accompanying magnetic field present for oscillating fields amounts to:

$$\mathbf{H} = \frac{i\omega}{4\pi} (\mathbf{n} \times \mathbf{p}) \frac{1}{r^2}.$$

We can see that within the near field, the fields are predominantly electric in nature, since the magnitude of the magnetic field is about a factor $\sqrt{(\varepsilon_0/\mu_0)}$ *(kr)* smaller than that of the electric field. For static fields *(kr → 0)*, the magnetic field vanishes.

In the opposite limit of the radiation zone, defined by *kr >> 1*, the dipole fields are of the well-known spherical-wave form:

$$\mathbf{H} = \frac{ck^2}{4\pi} (\mathbf{n} \times \mathbf{p}) \frac{e^{ikr}}{r}$$

$$\mathbf{E} = \sqrt{\frac{\mu_0}{\varepsilon_0\varepsilon_m}} \mathbf{H} \times \mathbf{n}.$$

We will now leave this short summary of the properties of dipolar radiation. It is much more interesting from the view point of optics to note that another consequence of the resonantly enhanced polarization α is a concomitant enhancement in the efficiency with which a metal nanoparticle scatters and absorbs light. The corresponding cross sections for scattering and absorption C_{sca} and C_{abs} can be calculated via the Poynting-vector determined from above [Bohren and Huffman, 1983] to:

$$C_{sca} = \frac{k^4}{6\pi} |\alpha|^2 = \frac{8\pi}{3} k^4 a^6 \left| \frac{\varepsilon - \varepsilon_m}{\varepsilon + 2\varepsilon_m} \right|^2$$

$$C_{abs} = k\text{Im}[\alpha] = 4\pi ka^3 \text{Im}\left[\frac{\varepsilon - \varepsilon_m}{\varepsilon + 2\varepsilon_m}\right].$$

For small particles with $a \ll \lambda$, the efficiency of absorption scaling with a^3, dominates over the scattering efficiency, which scales with a^6. We point out that no explicit assumptions were made in our derivations so far that the sphere is indeed metallic. The expressions for the cross sections are thus valid also for the dielectric scatterers, and demonstrate a very important problem for practical purposes. Due to rapid scaling of $C_{sca} \propto a^6$, it is very difficult to pick out small objects from a background of larger scatterers. Imaging of nanoparticles with dimensions below 40 nm, are immersed in an background of light scatterers can thus usually only be achieved using photo-thermal techniques relying on the slower scaling of the absorption cross section with size. Equations also show that indeed for metal nanoparticles, both absorption and scattering (and thus extinction) are resonantly enhanced at the dipole particle plasmon resonance, i.e. when Frölich condition is met. For a sphere of volume V and dielectric function $\varepsilon = \varepsilon_1 + i\varepsilon_2$ in the Quais-Statc limit, the explicit expression for the extinction cross section $C_{ext} = C_{abs} + C_{sca}$ is:

$$C_{ext} = 9\frac{\omega}{c}\varepsilon_m^{3/2} V \frac{\varepsilon_2}{[\varepsilon_1 + 2\varepsilon_m]^2 + \varepsilon_2^2}.$$
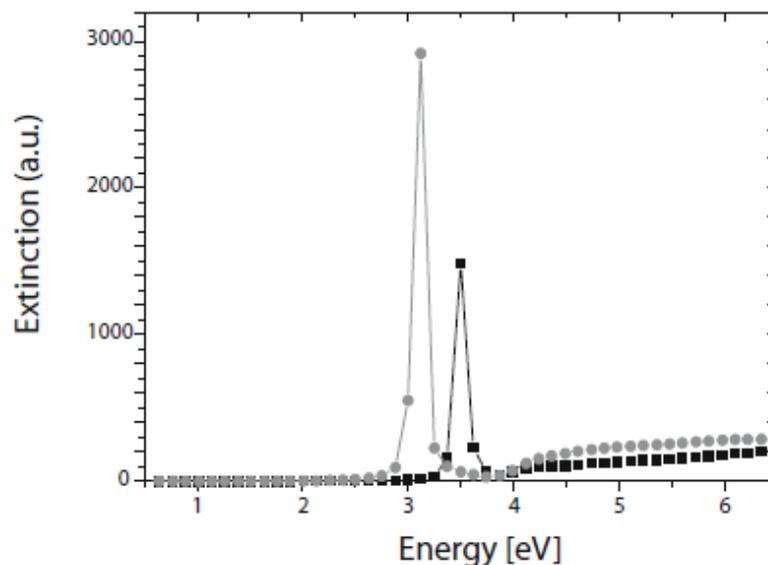
Figure 2.8 *Extinction cross section for a sliver sphere in air (black curve) and in silica (grey curve), with the dielectric data taken from [Johnson and Christy, 1972]* [5]

The above figure shows the extinction cross section of a sliver sphere in the Quasi-Static approximation calculated using this formula for immersion in two different media [5].

2.6 Difference between SPR and LSPR

Localized Surface Plasmon Resonance is produced by metal nanoparticles, especially silver and gold, whereas, Surface Plasmon Resonance is produced by a continuous film of gold.

Open SPR is comparable from multiple points of view to conventional SPR, and gives similar information utilizing the same exploratory conditions and systems. To the client, everything would appear the same between other SPR instruments and Open SPR. In any case, Open SPR utilizes what is known as Localized Surface Plasmon Resonance (LSPR).

LSPR produces a solid resonance absorbance peak in the visible range of light, with its position being exceptionally sensitive to the nearby refractive index encircling the molecule. In this manner, LSPR measures little changes in the wavelength of the absorbance position, as opposed to the angle as in conventional SPR [9].
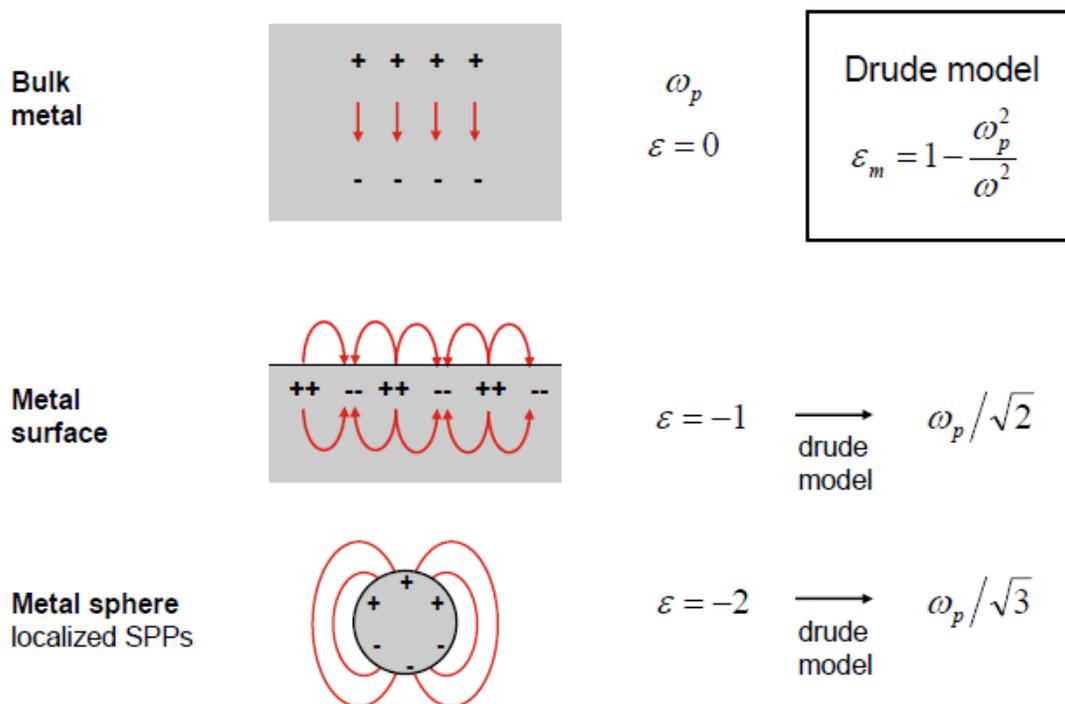
Figure 2.9 *Plasmon resonance positions in vacuum* [8]

Advantages of LSPR over SPR:

- The optical equipment required for LSPR is a great deal less perplexing since no prism is expected to couple the light, making the instrument smaller and more affordable

- Since the angle is not essential, the instrument is considerably heartier against vibration and mechanical noise

- LSPR is not as sensitive to bulk refractive index changes, which causes mistakes in experimental information, since it has a much shorter electromagnetic field decay length

- No strict temperature control is required, making the instrument simpler to use

- The sensor chips can be made at a more reasonable cost

- Easier to use and sustain
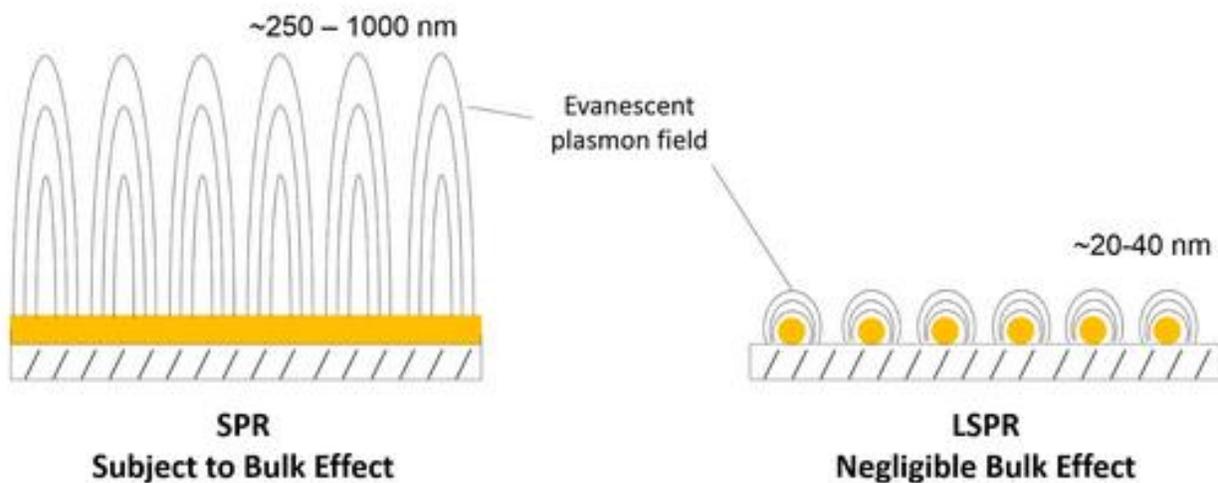
Figure 2.10 *The difference between SPR and LSPR for bulk effect* [9]

2.7 Drude-Sommerfield Model / Free Electron Model

In solid-state physics, the free electron model is a simple model for the behavior of valence electrons in a crystal structure of a metallic solid. It was developed primarily by Arnold Sommerfield, who combined the classical Drude Model with quantum mechanical Fermi-Dirac statistics and hence, it is also known as the **Drude-Sommerfield Model**.

The free electron empty lattice approximation forms the basis of the band structure model known as nearly free electron model. Given its simplicity, it is surprisingly successful in explaining many experimental phenomena, especially:

- the Wiedemann–Franz law which relates electrical conductivity and thermal conductivity;
- the temperature dependence of the heat capacity;
- the shape of the electronic density of states;
- the range of binding energy values;
- electrical conductivities;
- thermal electron emission and field electron emission from bulk metals.

Similar to the Drude Model, valence electrons are assumed to be entirely separated from their iond, forming an electron gas. Similar to the properties of an ideal gas, electron-electron interactions are completely ignored. The electrostatic fields are weak in metals because of the screening effect.

The crystal lattice is not clearly taken under consideration. A quantum-mechanical explanation is given by Bloch's Theorem: an unbound electron moves in a periodic potential as a free electron in vacuum, except for the electron mass m becoming an effective mass $m*$ which may deviate considerably from m It is even possible to use negative effective mass to describe conduction by electron holes. Effective masses can be derived from band structure computations. Even though the static lattice does not hamper the motion of the electrons, the electrons can be scattered by phonons and by impurities. These two determine the electrical and thermal conductivity (superconductivity requires a more refined theory than the free electron model).

According to the Pauli exclusion principle, each phase space element $(\Delta k)^3 (\Delta x)^3$ can be occupied only by two electrons (one per spin quantum number). This restriction of available electron states is taken into account by Fermi–Dirac statistics (see also Fermi gas). Main predictions of the free-electron model are derived by the Sommerfeld expansion of the Fermi–Dirac occupancy for energies around the Fermi level.

Energy and Wave Function of a Free Electron

For a free particle the potential is V(R) = 0. The Schrödinger equation for such a particle, like the free electron, is:

$$-\frac{\hbar^2}{2m}\nabla^2\Psi(\mathbf{r},t) = i\hbar\frac{\partial}{\partial t}\Psi(\mathbf{r},t)$$

The wave function ψ(r,t) can be split into a solution of a time dependent and a solution of a time independent equation. The solution of the time dependent equation is:

$$\Psi(\mathbf{r},t) = \psi(\mathbf{r})e^{-i\omega t}$$

With energy,

$$E = \hbar\omega$$

The solution of the time independent equation is:

$$\psi_{\mathbf{k}}(\mathbf{r}) = \frac{1}{\sqrt{\Omega_r}}e^{i\mathbf{k}\cdot\mathbf{r}}$$

With a wave vector k.Ω_r is the volume of space where the electron can be found. The electron has a kinetic energy:

$$E = \frac{\hbar^2 k^2}{2m}$$

The plane wave solution of this Schrödinger equation is:

$$\Psi(\mathbf{r},t) = \frac{1}{\sqrt{\Omega_r}}e^{i\mathbf{k}\cdot\mathbf{r}-i\omega t}$$

For solid state and condensed matter physics, the time independent solution $\psi_k(r)$ is extremely intriguing. It is the basis of electronic band structure models that are widely used in solid-state physics for model Hamiltonians like the nearly free electron model and the Tight binding model and different models that use a Muffin-tin approximation. The Eigen functions of these Hamiltonians are Bloch waves which are modulated plane waves [10].

2.8 Summary

Surface plasmon resonance is the resonant oscillation of conduction electrons at the interface between negative ($\varepsilon_m < 0$) and positive ($\varepsilon_d > 0$) permittivity material stimulated by incident light. Upon incidence of light whose frequency matches with that of the natural frequency of the conduction electrons, the oscillation of the conduction electrons in the metal and dielectric interface generates a propagating evanescent wave. The electric field propagates both inside and outside the metal. The generation of evanescent waves proves that the energy is confined in a small area where the light has hit the metal surface.

A Localized Surface Plasmon Resonance (LSPR) is the result of the confinement of a surface plasmon in a nanoparticle of size comparable or smaller than the wavelength of the light in the visible range or the light used to excite the plasmon. Unlike Surface Plasmons, Localized Surface Plasmons are **non-propagating** excitations of the conduction electrons of metallic nanostructures coupled to the electromagnetic field. These modes naturally generate an oscillating electromagnetic field from the scattering problem of a small, sub-wavelength conductive nanoparticle. As a result, a resonance arises, leading to field amplification on both inside and in the near-field zone outside the particle. This resonance is called **localized surface plasmon resonance**.

The advantages of LSPR over SPR include:

- High molecular sensitivity
- Simplicity of instrumentation
- Cost effectiveness

For gold and silver nanoparticles, the resonance falls into the visible range of the electromagnetic spectrum. It is solely because of this that the bright colors are displayed by particles both in transmitted and reflected light, due to resonantly improved absorption and scattering. This application has made itself very useful for many centuries, for example, in the staining of glass in windows or ornamental cups.

3. Bimetallic Core-Shell Nanoparticle Biosensors

3.1 Proposed Structure

The idea of the thesis is to carry out our research with a gold core and a sliver shell nanoparticle placed on top of a substrate (for example, SiO_2). The substrate and the nanoparticle are immersed in water and the entire setup is illuminated with light. We will observe the power absorbed by the particle, the electric field coupling and the SPR shift for different conditions and parameters. The experimental setup is shown below:
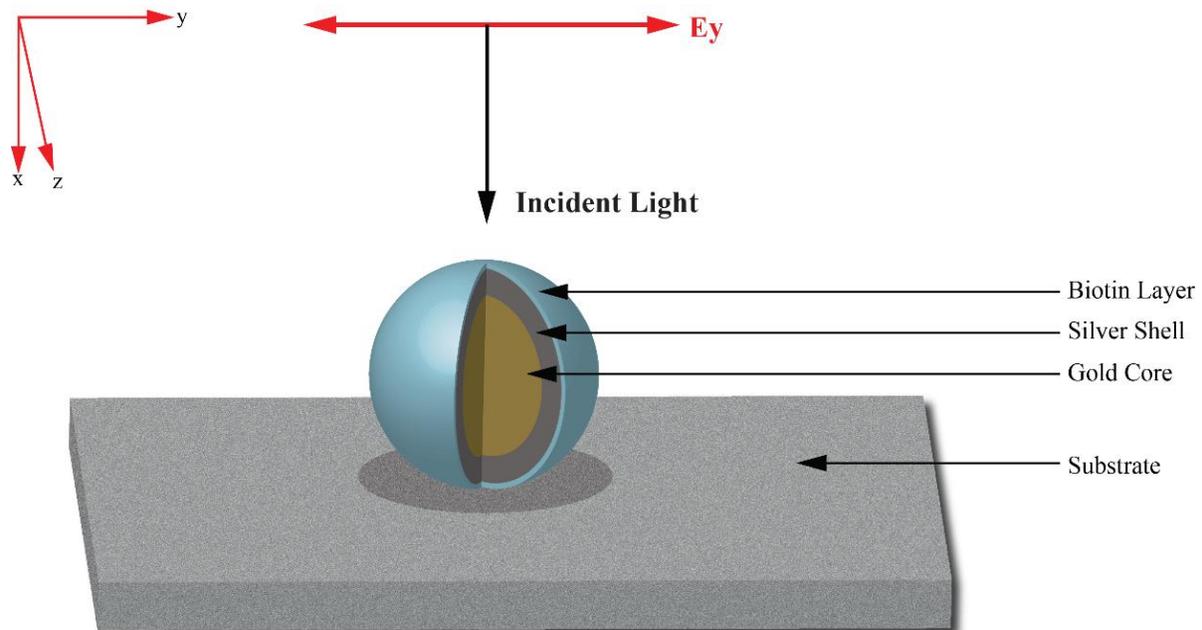
Figure 3.1 *Experimental Setup*

At first, we will observe the power absorption curve and the electric field coupling by varying the dimensions of the nanoparticle, i.e. the core radius and the coating shell length, whilst keeping all other variables constant, i.e. the substance used as the substrate (Silicon Dioxide) and the medium for refractive index (water). This part of the research is only based on the core-shell ratio.

Next, we will repeat the simulation with the same substrate and the same medium. However, we will not be concerned about the core-shell ratio. Instead, we will focus on the aspect ratio. This is where the coating shell will remain fixed at a particular value. Only the core radius will be varied and the corresponding power absorption curve and the electric field coupling will be analyzed.

The latter part of the research will focus on the sensitivity of the biomolecule. The dimensions of the nanoparticle will be fixed with two distinctive values of the core radii and coating lengths. For a particular set of the core-shell value, the surrounding medium will be changed, thus, changing the refractive index, and the corresponding sensitivity curve and the SPR Shift curve will be obtained and analyzed. Finally, the simulation will be repeated with the other core-shell value and the two obtained curves will be analyzed.

The final part of our research will deal with the substrate effect. Here, we will change the Silicon Dioxide substrate and replace it with Titanium Dioxide substrate and compare and analyze the SPR Shift due to the two materials.

3.2 Protein as a Biomolecule

A biomolecule or biological molecule is any sort of a molecule that is present in living organisms. These may include large molecules such as carbohydrates, proteins, starch, lipids and nucleic acids, and may also include small molecules such as primary metabolites, secondary metabolites and natural products. A more universal name for this type of material is biological material. Biomolecules are usually endogenous but may also be exogenous. For example, pharmaceutical drugs may be natural or semisynthetic (biopharmaceuticals) or they may be totally synthetic.

Biology and its subgroups of biochemistry and molecular biology research biomolecules and their reactions. Most molecules are organic compounds, and are comprised of just four elements: oxygen, carbon, nitrogen and hydrogen. They are responsible for 96% of the human body's mass. However, many other elements, such as various bio-metals are present in small amounts [11].

The biomolecules that we have used for our thesis paper have been mentioned below along with their refractive indices:

- Lysozyme (Lys) – Refractive index 1.5
- Human Serum Albumin (HSA) – Refractive index 1.45
- Human Immunoglobulin G (IgG) – Refractive index 1.41

3.2.1 Lysozyme (Lys)

Lysozymes, also known as muramidase or N-acetylmuramide glycanhydrolase, are glycoside hydrolases. These are enzymes (EC 3.2.1.17) that damage bacterial cell walls by catalyzing hydrolysis of 1,4-beta-linkages between N-acetylmuramic acid and N-acetyl-D-glucosamine residues in a peptidoglycan and between N-acetyl-D-glucosamine residues in chitodextrins. Lysozyme is abundant in a number of secretions, such as tears, saliva, human milk, and mucus. It is also present in cytoplasmic granules of the macrophages and the polymorphonuclear neutrophils (PMNs). Large amounts of lysozyme can be found in egg white. C-type lysozymes are closely related to alpha-lactalbumin in sequence and structure, making them part of the same family. In humans, the lysozyme enzyme is encoded by the *LYZ* gene.

The enzyme functions by attacking peptidoglycans (found in the cell walls of bacteria, especially Gram-positive bacteria) and hydrolyzing the glycosidic bond that connects *N*-acetylmuramic acid with the fourth carbon atom of N-acetylglucosamine. It does this by binding to the peptidoglycan molecule in the binding site within the prominent cleft between its two domains. This causes the substrate molecule to adopt a strained conformation similar to that of the transition state. According to Phillips-Mechanism, the lysozyme binds to a hexasaccharide. The lysozyme then distorts the fourth sugar in hexasaccharide (the D ring) into a half-chair conformation. In this stressed state, the glycosidic bond is easily broken [12].
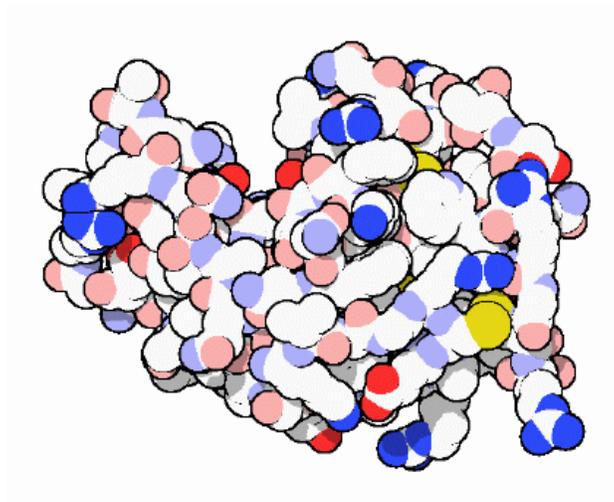
Figure 3.2 *Lysozyme* [16]

3.2.2 Human Serum Albumin (HSA)

It is the version of serum albumin found in human blood. HSA is the most plentiful protein in human blood plasma and it sets up about half of plasma serum protein. It is produced in the liver. HSA is soluble and monomeric (a molecule that can combine with other molecules to form a polymer). Albumin transports hormones, fatty acids, and other compounds, buffers pH, and maintains oncotic pressure, among other functions.

Albumin is synthesized in the liver as preproalbumin, which has an N-terminal peptide that is removed before the nascent protein is released from the rough endoplasmic reticulum. The product, proalbumin, is in turn cleaved in the Golgi vesicles to produce the secreted albumin.

The reference range for albumin concentrations in serum is approximately 35 - 50 g/L (3.5 - 5.0 g/dL). It has a serum half-life of approximately 20 days. It has a molecular mass of 66.5 kDa.

The gene for albumin is located on chromosome 4 and mutations in this gene can result in anomalous proteins. The human albumin gene is 16,961 nucleotides long from the putative 'cap' site to the first poly (A) addition site. It is split into 15 exons that are symmetrically placed within the 3 domains thought to have arisen by triplication of a single primordial domain [13].
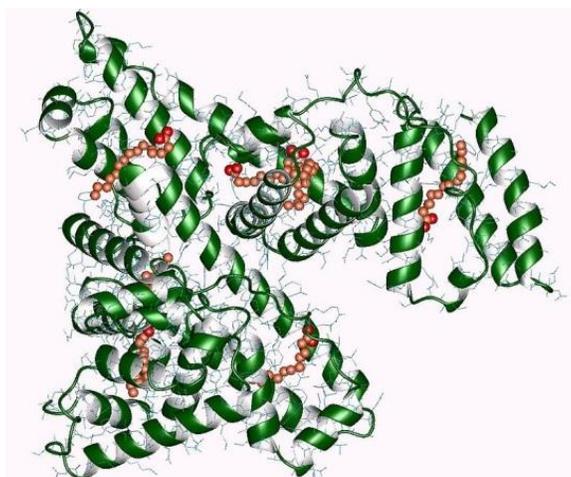
Figure 3.3 *Human Serum Albumin* [13]

3.2.3 Human γ-immunoglobulin (IgG)

Immunoglobulin G (IgG) is a type of antibody. It is a protein complex composed of four peptide chains: two identical heavy chains and two identical light chains arranged in a Y-shape typical of antibody monomers. Each immunoglobulin G molecule has two antigen binding sites. IgG is the most common type of antibody found in the circulation and is responsible for approximately 75% of serum antibodies in humans. IgG molecules are created and released by plasma B cells.

Antibodies are major components of humoral immunity. IgG is the main type of antibody found in blood and extracellular fluid. This causes it to control infection of body tissues. By binding many kinds of pathogens such as viruses, bacteria, and fungi, IgG protects the body from infection.

It does this through several mechanisms:

- IgG-mediated binding of pathogens causes their immobilization and binding together via agglutination; IgG coating of pathogen surfaces (known as opsonization) allows their recognition and ingestion by phagocytic immune cells leading to the elimination of the pathogen itself;
- IgG activates the classical pathway of the complement system, a cascade of immune protein production that results in pathogen elimination;
- IgG also binds and neutralizes toxins;
- IgG also plays an important role in antibody-dependent cell-mediated cytotoxicity (ADCC) and intracellular antibody-mediated proteolysis, in which it binds to TRIM21 (the receptor with greatest affinity to IgG in humans) in order to direct marked virions to the proteasome in the cytosol.;[2]
- IgG is also associated with type II and type III hypersensitivity reactions.

IgG antibodies are generated following class switching and maturation of the antibody response and thus participate primarily in the secondary immune response. IgG is secreted as a monomer that is small in size allowing it to easily penetrate tissues. It provides protection to the fetus in the utero since it is the only isotope that has receptors to create passages through the human placenta. Along with Immunoglobulin A (IgA) secreted in the breast milk, residual IgG absorbed through the placenta provides the neonate with humoral immunity before its own immune system develops. Colostrum contains a high percentage of IgG, especially bovine colostrum. In individuals with prior immunity to a pathogen, IgG appears about 24–48 hours after antigenic stimulation.

Hence, in the first six months of life, the fetus has the same antibodies as the mother, till the old antibodies are then degraded and he can defend himself against all the pathogens that the mother came across in her life (even if only through vaccination). This selection of immunoglobulin is crucial for the newborns who are very sensitive to infections above all for the respiratory and digestive systems.

It is also confirmed that in adults, the production of IgG is linked to the nutritional dominance of a specific food or food-group in the personal diet. As a result, the levels of IgG for food reflect dietary intake or express a possible previous immune contact with food. The total IgG values towards specific foods indicate excessive or repetitive consumption of them. IgG are also involved in the regulation of allergic reactions. According to Finkelman, there are two pathways of systemic anaphylaxis: antigens can cause systemic anaphylaxis in mice through classic pathway by cross-linking Immunoglobulin E (IgE) bound the mast cell FcεRI, stimulating histamine and PAF release. In the Alternative pathway antigens form complexes with IgG that cross-link macrophage Fc γ RIII, stimulating only PAF release.

IgG antibodies can prevent IgE mediated anaphylaxis by interrupting a specific antigen before it binds to mast cell associated with IgE. Consequently, IgG antibodies block systemic anaphylaxis induced by small quantities of antigen but can intercede systemic anaphylaxis induced by larger quantities [14].
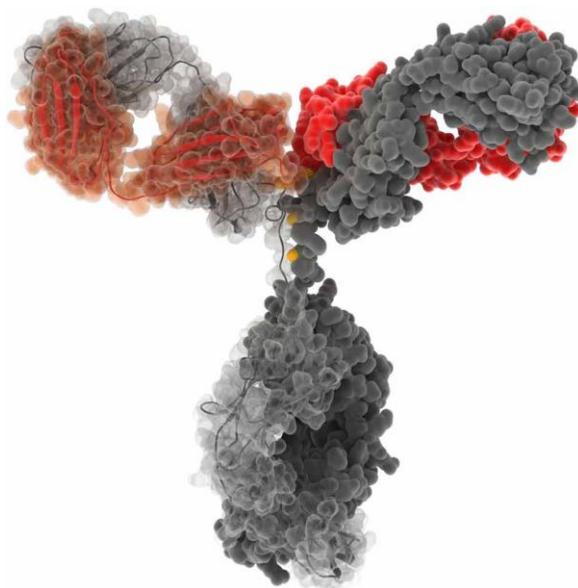

Figure 3.4 *Human Immunoglobulin G* [17]

3.3 Summary

Any sort of molecule that is present in living beings is known as a biomolecule or a biological molecule. Examples include large molecules like carbohydrates, proteins, starch, lipids etc., and may also include small molecules like primary and secondary metabolites, and natural products. Biological material is a more universal name for such materials. Biomolecules and their reactions are topics of interest and research in biology and biochemistry. Most of the molecules are organic compounds and their basic structures consist just four elements: oxygen, carbon, nitrogen and hydrogen. 96% of the human body's mass is the result of these elements.

Lysozymes, also known as muramidase or N-acetylmuramide glycanhydrolase, are glycoside hydrolases. These are enzymes (EC 3.2.1.17) that damage bacterial cell walls by catalyzing hydrolysis of 1,4-beta-linkages between N-acetylmuramic acid and N-acetyl-D-glucosamine residues in a peptidoglycan and between N-acetyl-D-glucosamine residues in chitodextrins. Lysozyme is abundant in a number of secretions, such as tears, saliva, human milk, and mucus. It is also present in cytoplasmic granules of the macrophages and the polymorphonuclear neutrophils (PMNs). Large amounts of lysozyme can be found in egg white. C-type lysozymes are closely related to alpha-lactalbumin in sequence and structure, making them part of the same family. In humans, the lysozyme enzyme is encoded by the *LYZ* gene.

The refractive index of Lysozyme is 1.5.

Human Serum Albumin is the version of serum albumin found in human blood. HSA is the most plentiful protein in human blood plasma and it sets up about half of plasma serum protein. It is produced in the liver. HSA is soluble and monomeric (a molecule that can combine with other molecules to form a polymer). Albumin transports hormones, fatty acids, and other compounds, buffers pH, and maintains oncotic pressure, among other functions.

The refractive index of Human Serum Albumin is 1.45.

Immunoglobulin G (IgG) is a type of antibody. It is a protein complex composed of four peptide chains: two identical heavy chains and two identical light chains arranged in a Y-shape typical of antibody monomers. Each immunoglobulin G molecule has two antigen binding sites. IgG is the most common type of antibody found in the circulation and is responsible for approximately 75% of serum antibodies in humans. IgG molecules are created and released by plasma B cells.

The refractive index of Immunoglobulin G is 1.41.

4. FDTD Solutions

4.1 Introduction

We are trying to create a spherical bimetallic nanoparticle which is composed of a gold core and a silver shell in the nanometer range. The nanoparticle is placed on a Silicon Dioxide (SiO_2) substrate. The setup illuminated with light and we observe the Power Absorption curve of the nanoparticle. Furthermore, we analyze the electric field coupling of the **Ordinary** Plasmon Resonance as well as the **Extraordinary** Plasmon Resonance.

4.1.1 Ordinary Plasmon Resonance

Ordinary plasmon resonances are the plasmons that are generated in the outer surface of the core-shell nanoparticle. This phenomenon is observed in single as well as bimetallic nanoparticles. Ordinary plasmon resonance is found in the peak points of the P_{abs} curve. Different peaks of the P_{abs} curve give us different values of the field coupling. Each of the peak values are given a unique name. We have found curves with two peak values in our results: we are assuming the highest value of the peak to be First Order Ordinary and the second one to be Higher Order Ordinary. These peak values are also called Longitudinal SP and Transverse SP respectively. In the First Order Ordinary, the value of the electric field coupling is highest compared to the rest of the peak values. However, even though the coupling is highest in the First Order Ordinary, we get better coupled electric field for Higher Order Ordinary.
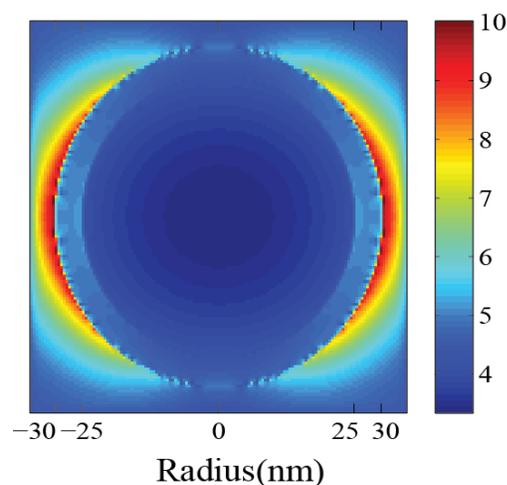
Figure 4.1 *Electric Field coupling for Ordinary Plasmon Resonance*

4.1.2 Extraordinary Plasmon Resonance

Extraordinary plasmon resonance are the plasmons that are generated in the interface between the two metal layers; they are not found everywhere. It is only bimetallic molecules that can create this phenomenon. The extraordinary point is usually found in the minimum value between the First Order Ordinary and Higher Order Ordinary peaks. The electric field coupling for extraordinary plasmons is greater than the field coupling of Higher Order Ordinary but lower than First Order Ordinary.
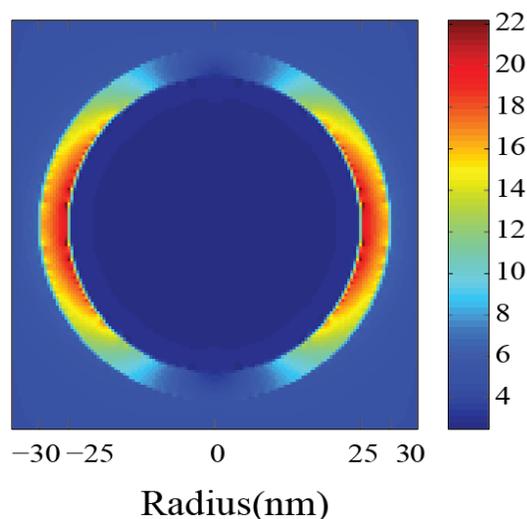
Figure 4.2 *Electric Field coupling for Extraordinary Plasmon Resonance*

We can only get the Extraordinary Plasmon Resonance when we use Gold as the core and Silver as the shell. However, it does not work the other way around. This is because Gold is a very stable metal compared to Silver. Therefore, if Silver is used as the core, its generated SPR might be blocked by the Gold shell. As a result, the SPR of Silver might not be detected at all. On the contrary, if Gold is used as the center, the SPR generated from within can penetrate the Silver shell and can be detected. Hence, Gold is used as the core and Silver is used as the shell.

4.2 About Lumerical

The name **Lumerical** is a mixture of two words: **Luminous** (full of light, illuminated) and **Numerical** (of or relating to a number or a series of numbers).

Figure 4.3 *Lumerical Logo* [19]

Lumerical develops photonic simulation software – tools which enable product designers to understand light, and predict how it behaves within complex circuits, structures and systems. Photonics is the study of light and its interaction with matter, and it unravels many opportunities for the world's leading technology companies across various fields including biotechnology, data communications, information storage, solar energy, environmental sensing and consumer electronics [15].

4.3 Material modeling

At first the software is installed and opened. Four windows appear on the screen, each with a significance of its own. The top left window shows the xy plane, the bottom left window shows the xz plane, the bottom right window shows the yz plane and the top right window displays the 3D (xyz) illustration of the particle.

Initially, we go to "Settings" and set the length unit to nanometers since we are dealing with nanoparticles. Then we insert the nanoparticle by following these instructions: Components > Ellipsoid > Coated Sphere. We insert the coated sphere in order to simulate two metals, i.e. a gold core and a silver shell.

Next, we go to the "coated_sphere" option and select the "edit object" option in order to set the dimensions of the nanoparticle. We find a box where we can change the mat coating, index coating, material, radius etc. according to our specifications. We changed the mat coating and selected Ag (Silver) – Johnson and Christy. The length (h coating) is varied from 5 nm to 15 nm. We have changed the material for the core and selected Au (Gold) – Johnson and Christy. The radius is varied from 10 nm to 25 nm.

The nanoparticle is coated with a Biotin Layer of 1 nm. This layer acts as an adhesive where biomolecules get stuck to the surface. In simple words, Biotin Layer acts as a glue.
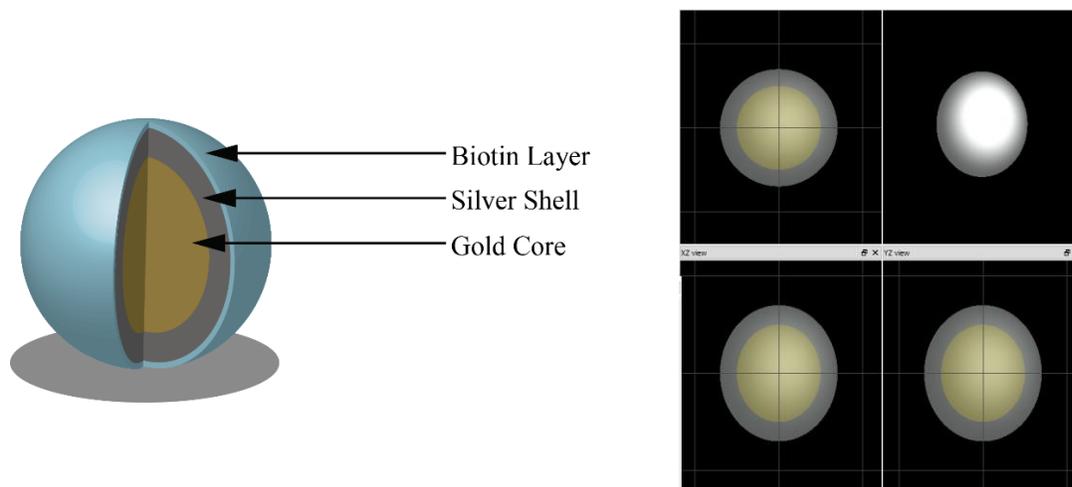
Figure 4.4 *(a) Model of the Bimetallic Nanoparticle (b) Schematic of the Bimetallic Nanoparticle*

4.4 FDTD - Finite Difference Time Domain

FDTD allows us to change the surroundings of the nanoparticle to create the experimental setup to ensure the proper conditions required for our thesis research.

4.4.1 General

We go to "Simulation > Region > General". An option appears under "coated_sphere" named "FDTD". We edit the object by setting the value of the "background index" to 1.33 to match the refractive index of water. This ensures that the nanoparticle is completely immersed in water. The "Simulation time" is set to 300. If the simulation time set to a large value, the size of the file increases highly and it takes a very long time to obtain he results. If we set the simulation time to a small value, we will not get the desired results. Hence, we have selected an optimum value of 300 fs.

4.4.2 Geometry

Now, we have selected the "Geometry" option located right next to "General". There are six options: x (nm), y (nm), z (nm), x span (nm), y span (nm) and z span (nm). The values of x, y and z are set to 0. This ensures that the simulation will occur over a range and not over a fixed value. That is why we use the x, y, z span options. The value of each span we are setting is 200 nm. This means that FDTD is automatically taking the coated sphere as the center and there is a length of 100 nm in each direction (x, y, z) around the particle.

4.4.3 Boundary Conditions

The boundary conditions that are supported by FDTD/MODE Solutions, which we have used for our research, are listed below. The values of "x min bc" and "x max bc" have been set to PML. After we have set the value of "y min bc" to be Periodic, the value of "y max bc" automatically gets fixed to Periodic. Finally, "z min bc" is set to Symmetric and "z max bc" is set to PML. The applications and explanations of PML, Symmetric and Periodic are listed below.

4.4.3.1 Perfectly Matched Layers (PML)

By construction, PML absorbing boundary conditions are impedance matched to the simulation region and its materials. This allows them to absorb light waves (both propagating and evanescent) with minimal reflection. An ideal PML boundary produces zero reflections, however, in practice there will always be small reflections due to the decentralization of the underlying PML equations. Furthermore, as a consequence of using finite difference approximations to decentralize the PML equations, there is some chance of producing numerical instabilities. The goal of this section is to outline best practices for minimizing reflection errors and getting rid of numerical instabilities without increasing simulation times unnecessarily.
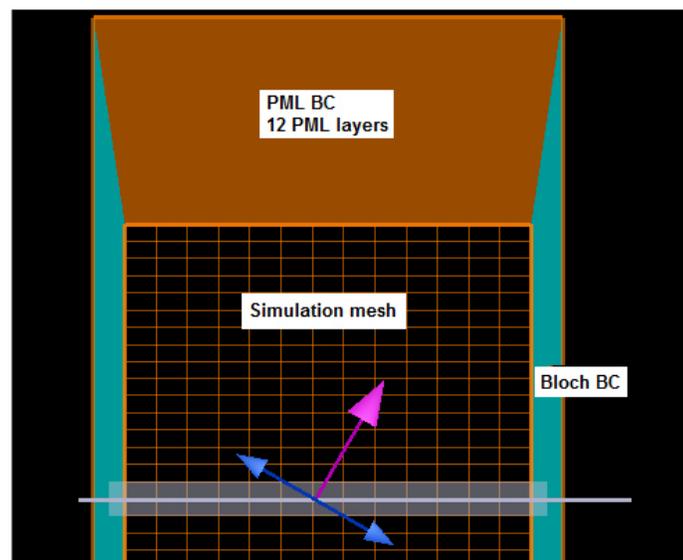
Figure 4.5 *Schematic of PML* [23]

4.4.3.2 Periodic

When studying periodic systems, Periodic BC's allow you to calculate the response of the entire system by only simulating one unit cell. Periodic BC's are relatively straightforward to use in the simulation: simply set the simulation span to be one unit cell wide and select Periodic BC's for that boundary. When the simulation runs, the Periodic BC's simply copy the EM fields that occur at one side of the simulation and inject them at the other side.

The most important detail to remember is that when using periodic BCs, everything in the system must be periodic: both the physical structure and the EM fields. A common source of error is to use periodic conditions in systems where the structure is periodic but EM fields are not.
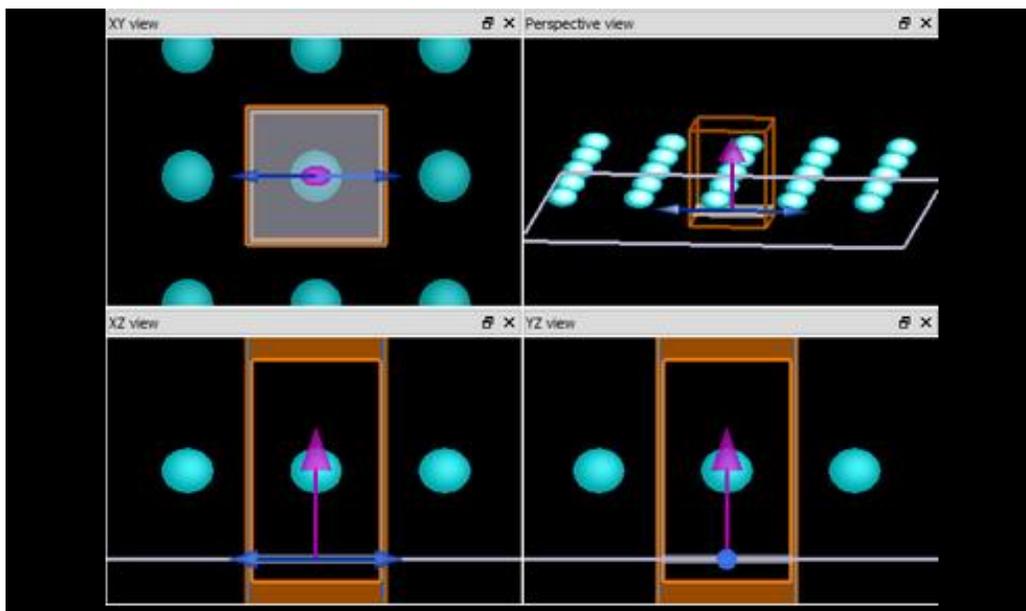
Figure 4.6 *Schematic of Periodic* [22]

The following sub-section will deal with the Symmetric Boundary Condition. In our simulation, Periodic and Symmetric performed the same operation to some extent.

4.4.3.3 Symmetric

Symmetric boundary condition can be used whenever the EM fields have a plane of symmetry through the middle of the simulation region. By taking advantage of this symmetry, the simulation volume and tie can be reduced by factors of 2, 4 or 8. This topic describes the difference between symmetric and anti-symmetric boundary conditions, and how to select the appropriate boundary of our simulation.
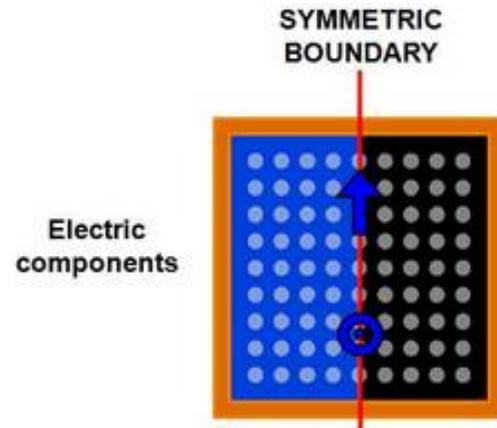
Figure 4.7 *Schematic of Symmetric* [21]

Rules of symmetry:

The electric and magnetic fields will obey certain symmetry rules with respect to reflections through the plane of symmetry. The reflection symmetry rules are shown in the figure to the right:
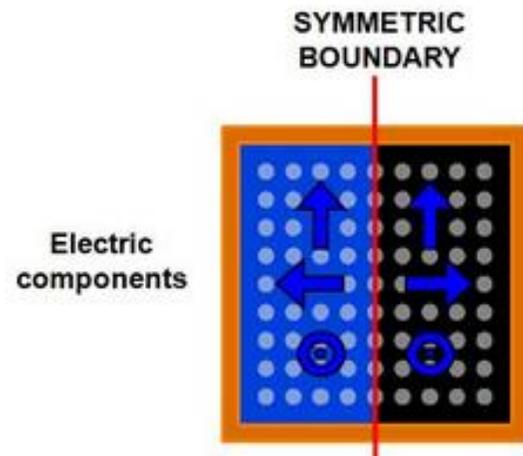
Figure 4.8 *Schematic of the rules of Symmetry* [21]

4.5 Mesh Analysis

After setting the conditions in FDTD, we can start with the mesh analysis. Accessibility of mesh is obtained from "Simulation > Mesh". The values of the "General" settings are set to 1 because lower values guarantee better accuracy. However, we do not take values less than 1, such as 0.5 or 0.25, because this increases the size of the file so much that the simulation time increases highly and after a few minutes into the simulation, the file shows an error and stops. We can only use 0.5 of the mesh value to get a smooth and good quality result for electric filed, but not the entire simulation.

In this application, we use a combination of graded meshing and conformal meshing. The conformal meshing allows us to obtain more accurate results for a given mesh size. Even if the mesh size is only twice as large, for example 2 nm compared to 1 nm, the computation time in 3D simulations can be reduced by a factor of 16. We need to be careful when using conformal mesh technology with metals, however, and do some convergence testing to be sure that the conformal mesh technology is appropriate for your precise application.

Now, we have selected the "Geometry" option located right next to "General" (same as FDTD). There are six options: x (nm), y (nm), z (nm), x span (nm), y span (nm) and z span (nm). The values of x, y and z are set to 0. This ensures that the simulation will occur over a range and not over a fixed value. That is why we use the x, y, z span options. However, the value is chosen in a way such that the mesh just covers the nanosphere. The value of each span is set according to our requirements. For example, if the diameter of the particle is 30 nm, we set the value of the mesh geometry to be 35 nm. This means that FDTD is automatically taking the coated sphere as the center and there is a length of around 17.5 nm in each direction (x, y, z) around the particle.
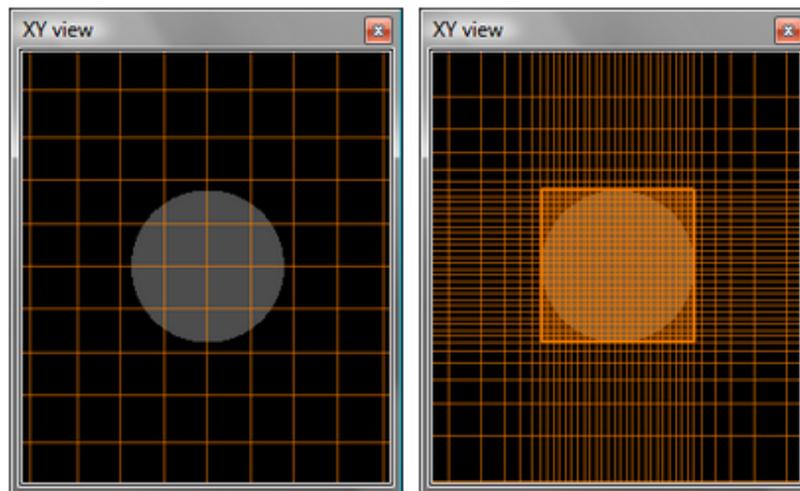
Figure 4.9 *Schematic of Mesh* [24]

4.6 Substrate Formation

Substrate is the structure on top of which the nanoparticle is placed; it is the bottom layer of the box. The substrate can be comprised of many different materials. For our case, the material that we are using is "SiO2 (Glass) – Palik". There are a few advantages behind our choice. First of all, SiO_2 is very cheap. It is basically sand glass. Secondly, it is easily available and most importantly, Silicon automatically creates a layer of SiO_2 on its surface by reacting with the Oxygen present in air.

In order to apply the substrate to our setup, we take the following directions "Structure > Rectangle". Then we edit this object according to our necessities; we change the "Geometry" of the rectangle. There are six options: x (nm), y (nm), z (nm), x span (nm), y span (nm) and z span (nm). The values of y and z are set to 0. The values of y and z spans are 400 nm each. The value of x is set to 115 nm and the value of x span is set to 200 nm because unlike y and z, we need not consider the positive and negative directions on either side of the nanoparticle. We are only concerned about the nanoparticle touching the substrate along the x direction.

Lastly, the substrate is rotated in the x direction because initially, the thickness was in the z direction, but for our case, the thickness is changed to the x direction.

The refractive index of Silicon Dioxide is 1.46.

Advantages of Silicon Dioxide:

- Outstanding thermal stability
- Low expense coefficient
- Compressive stress preload
- High strength (1 GPa) and stiffness
- Excellent thickness control
- Easily reworked die attach

4.7 Source

This is the light source that is being used to illuminate the entire experimental setup. With the purpose of adding a light source to our already existing apparatus, we follow "Sources > Total Field Scattered Field (TFSF)". This installs the light source in the setup. Now, the object is edited.

The "General" settings are altered with the injection axis set in the x direction (along the direction of the thickness). The amplitude is set to 5 for the ease of understanding.

As always, we change the "Geometry" of the rectangle. There are six options: x (nm), y (nm), z (nm), x span (nm), y span (nm) and z span (nm). The values of x, y and z are 0. The values of x, y and z spans are set according to our preferences. Not too large a value is chosen because it is unnecessary. We chose the values in such a way so that the light just covers the entire nanoparticle.

Now, we deal with the "Frequency/Wavelength" settings. The "Set frequency/wavelength" is kept constant because want the curve with respect to frequency, not time. At first, we have set the start and stop values of wavelength to be 0 and 1000 respectively. However, we observed that the entire range of this wavelength is not necessary for our setup because the peak value lies somewhere between 400nm and 600 nm. That is why we have chosen the range from 400 to 600 nm.
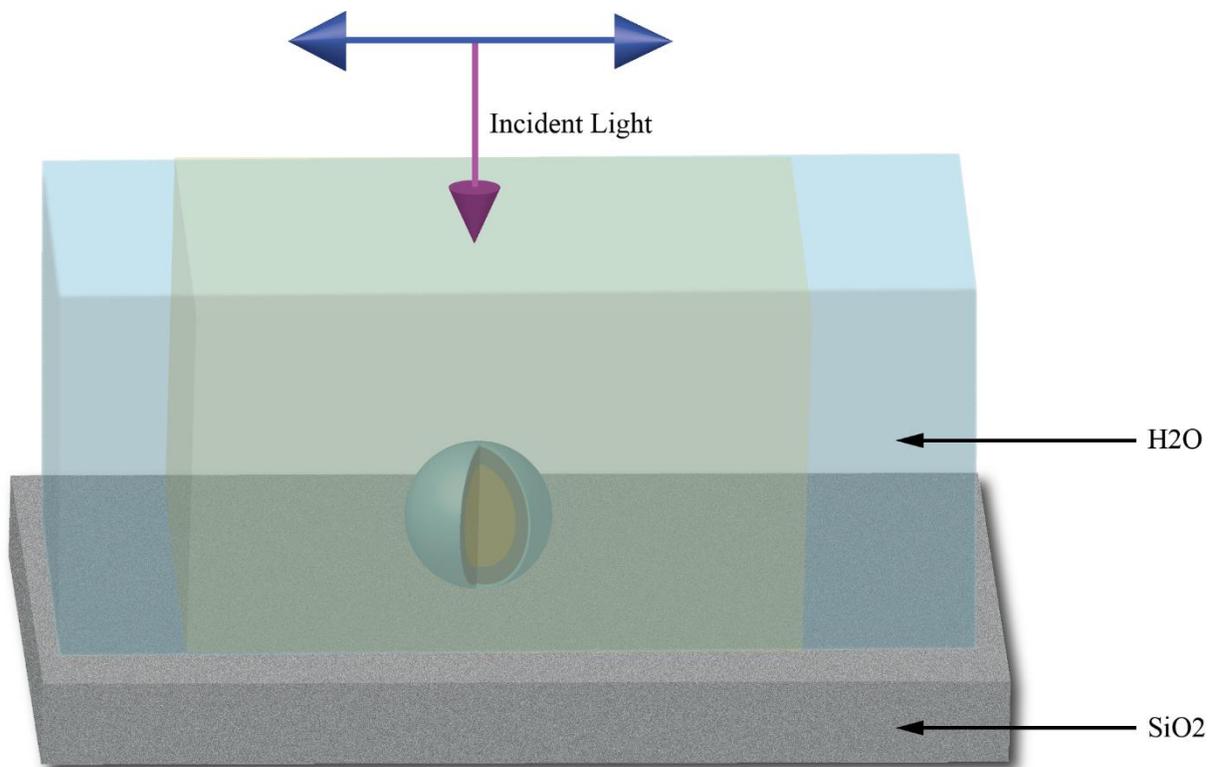
Figure 4.10 *Illustration of the experimental setup with the surrounding medium*

4.8 Power Absorption (Advanced)

This is the advanced version of power absorption. Power absorption is taken into account so that we can observe the amount of power absorbed after the simulation is done in a graphical format. In order to access this feature, we go to "Analysis > Optical Power > Power absorbed (advanced)".
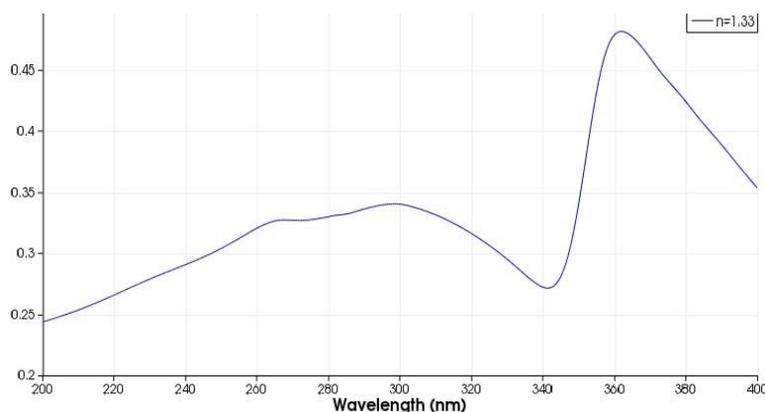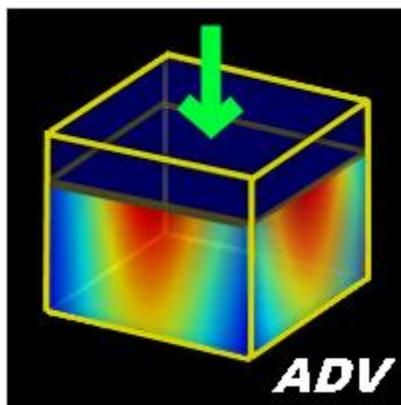
Figure 4.11 *Power Absorption Curve*

4.9 Monitor

We went to "Monitor > Frequency – domain field and power". This object is then edited. The "override global monitor settings" is checked out. This allows us to enter the value of frequency points. We change the frequency points with respect to our requirements.

Then we move on to the "Geometry". The Monitor Type is set to 2D X-normal (along the direction of the thickness of the substrate). X span automatically gets fixed to 0.

When we fix the wavelength at a particular point rather than a range, Monitor gives us the electric filed or magnetic field pictures.

4.10 Summary

Lumerical develops photonic simulation software – tools which enable product designers to understand light, and predict how it behaves within complex circuits, structures and systems. Photonics is the study of light and its interaction with matter, and it unravels many opportunities for the world's leading technology companies across various fields including biotechnology, data communications, information storage, solar energy, environmental sensing and consumer electronics.

We have used FDTD Solutions in our thesis paper in order to simulate and analyze the results obtained from bimetallic core-shell nanoparticles. We have accurately designed the surrounding, substrate material, direction of incident light and electric field for our research. The nanoparticle is made with the help of the "Coated_sphere" option. The General settings allow us to choose the material(s) the nanoparticle is to be made of and the dimensions of it. The FDTD option provides us with General, Geometry, Boundary Conditions and a lot more. However, we focus on these three only. In every part, Geometry allows us to vary the values of the boundary. General settings are used to vary the surroundings as well as the angles (or direction). Finally, Boundary Conditions allow us to simulate certain parts of the experimental setup. For instance, if we go for the Symmetric option, the software automatically simulates half of the setup, and arithmetically doubles the value and displays the total result. Mesh Analysis is used for smooth curves. The smaller the value of Mesh is, the smoother the curve will be. Substrate is the bottom layer for any kind of stricture. For our research, we have used Silicon Dioxide (SiO_2) as our substrate. For the source, we have used TFSF (Total Field Scattered Field) light. Finally, in order to check the results, we have used the P_{abs} (advanced) and the Monitor option. P_{abs} (advanced) is required for the analysis of the power absorption curve and Monitor is required for the electric filed coupling.

5. Simulation and Result Analysis

5.1 Introduction

After setting up the values and conditions required for our research, we began our simulation process. We have obtained Power Absorption curves. From those curves, we have obtained the Extraordinary, Ordinary and First Order points as well as their Electric Field Coupling pictures.

The results of the simulation have been categorized into four parts:
- Core-Shell Ratio
- Aspect Ratio
- Sensitivity of Biomolecule
- Substrate Effect

5.2 Core-Shell Ratio

The lengths of the gold core and the silver shell were varied simultaneously whilst keeping the total radius (core + shell) fixed at 30 nm. For example, if the length of the core is 5 nm, the radius of the shell will be 25 nm. The frequency of the incident light is 400 Hz. This is because we want to observe two points between two intervals. The value of Mesh is set to 1. Now, the setup is simulated for a fixed value of the core and shell to obtain the P_{abs} curve. From the curve, we record the values of the Ordinary, Extraordinary and the First Order points. The simulation is repeated for different values of the core and the shell and the corresponding Extraordinary, Ordinary and the First Order points (wavelengths of the incident light at which the resonances occur) are displayed in the table below:

Table of Results:

Core-Shell Ratio	Extraordinary/nm	Ordinary (Higher Order)/nm	First Order/nm
C-25, S- 5	321.081	264.000	364.384
C-20, S-10	328.081	262.445	379.097
C-15, S-15	318.789	262.445	385.510
C-10, S-20	318.789	260.900	387.379

Graphical Representation:
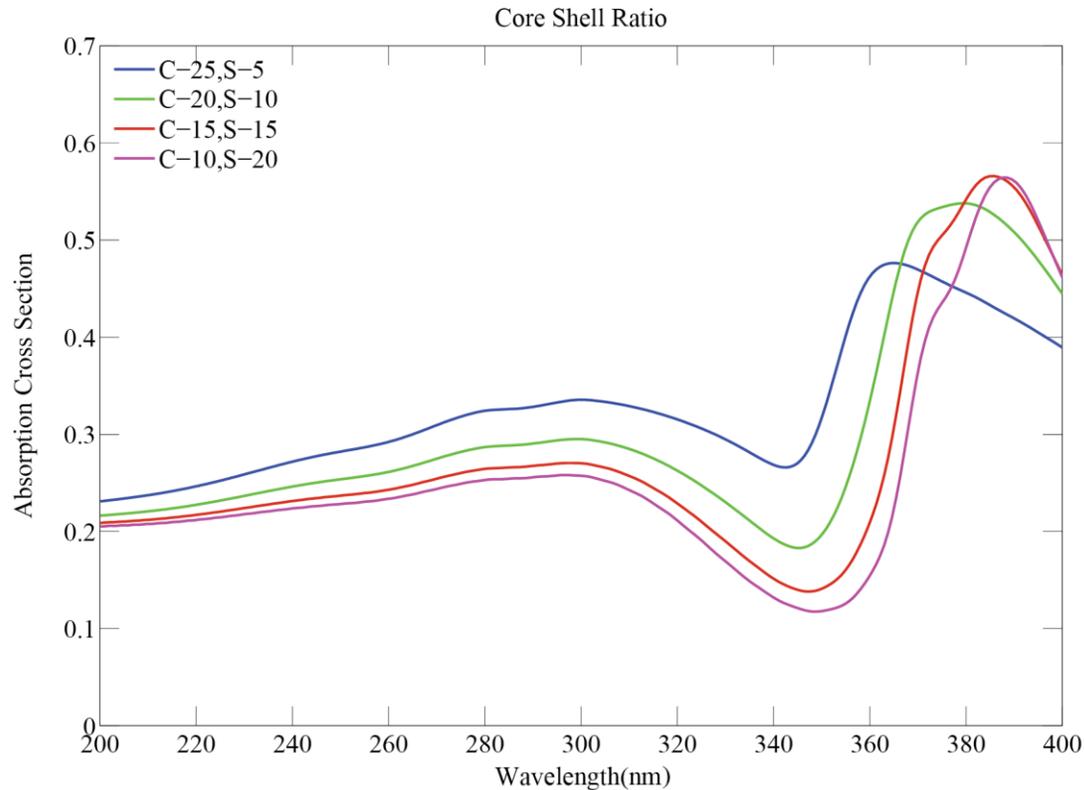
Figure 5.1 *Power Absorption curve of the Core-Shell Ratio*

The maximum point for each curve represents the First Order Values and the minimum points represent the Extraordinary values. The second maximum value represents the Higher Order Ordinary point for each curve. Upon increasing the core radius and decreasing the coating shell length, the power absorption increases for Extraordinary and Ordinary points. However, this is the opposite for the First Order Ordinary points. Moreover, the wavelength of the First Order Ordinary points shift by a greater amount compared to the Extraordinary and Ordinary points.

For each of the extraordinary, ordinary and the First Order points, we have observed the electric field coupling. This is done to compare how the field coupling changes with respect to the core-shell ratio.
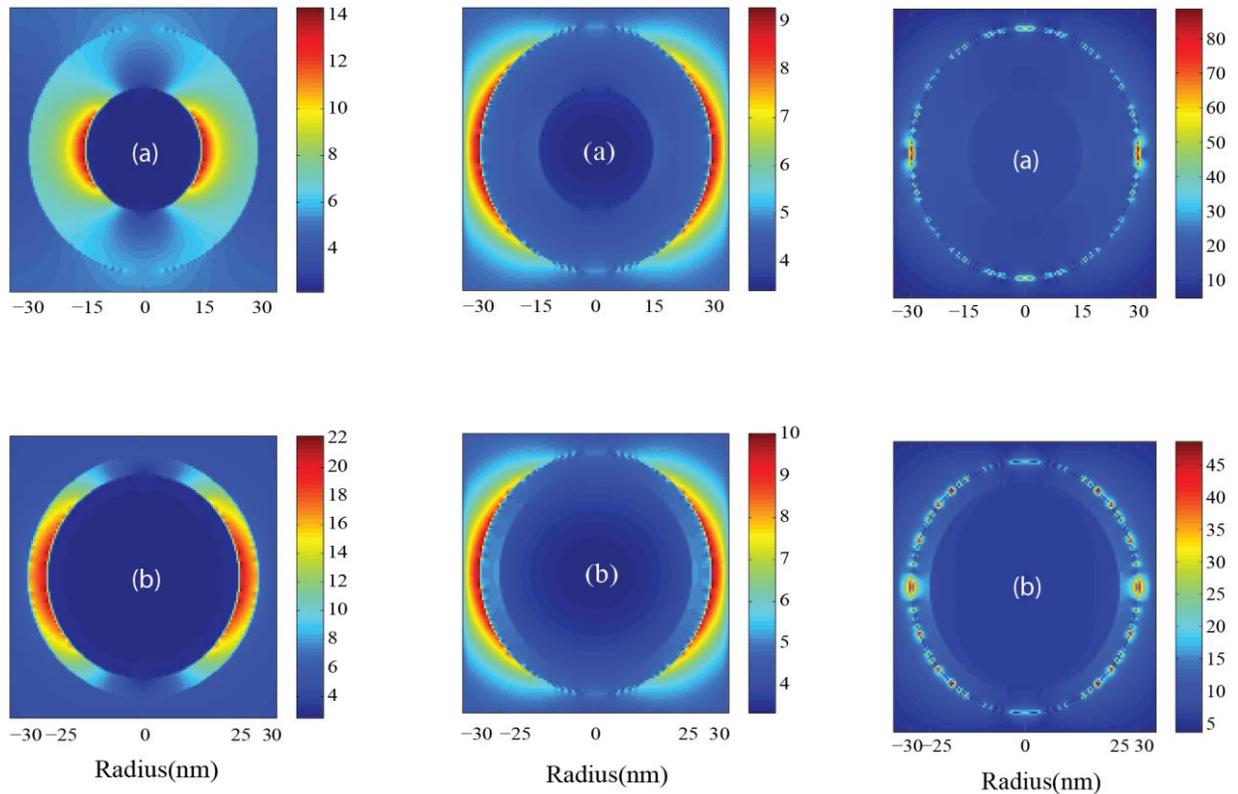
Figure 5.2 *Electric Field coupling diagram for Extraordinary, Ordinary and First Order Ordinary Plasmon Resonances respectively*

In the above figure, (a) represents C-15, S-15 and (b) represents C-25, S-5. For Extraordinary, it is seen that we have obtained effective coupling. It can also be deduced that the value of coupling increases as we increase the size of the core whilst decreasing the size of the shell, reaching a maximum value of 22 from 14 as we move from (a) to (b). For Ordinary, we are preferring the higher order peak value since the coupling is effective. While moving from (a) to (b), the maximum value of coupling increases. However, the change is not as significant as it is in Extraordinary (from a maximum value of 9 to a maximum value of 10). We are ignoring the First Order because although the coupling is high, the electric field is scattered.

5.3 Aspect Ratio

The coating of the silver shell is kept fixed at 5 nm while varying the radius of the gold core form 10 nm to 25 nm. The frequency of the incident light is 400 Hz. The value of the Mesh is set to 1. Now, the setup is simulated with the length of the shell fixed at 5 nm and a particular value of the core radius. P_{abs} curve is obtained and the corresponding points of Extraordinary, Ordinary and First Order are recorded. The simulation is repeated for different radii of the core and the data are displayed in the table below:

Table of Results:

Aspect Ratio	Extraordinary/nm	Ordinary (Higher Order)/nm	First Order/nm
C-10, S-5	339.574	288.610	367.742
C-15, S-5	340.298	291.773	364.380
C-20, S-5	341.026	293.923	362.727
C-25, S-5	321.081	264.000	364.384

Graphical Representation:
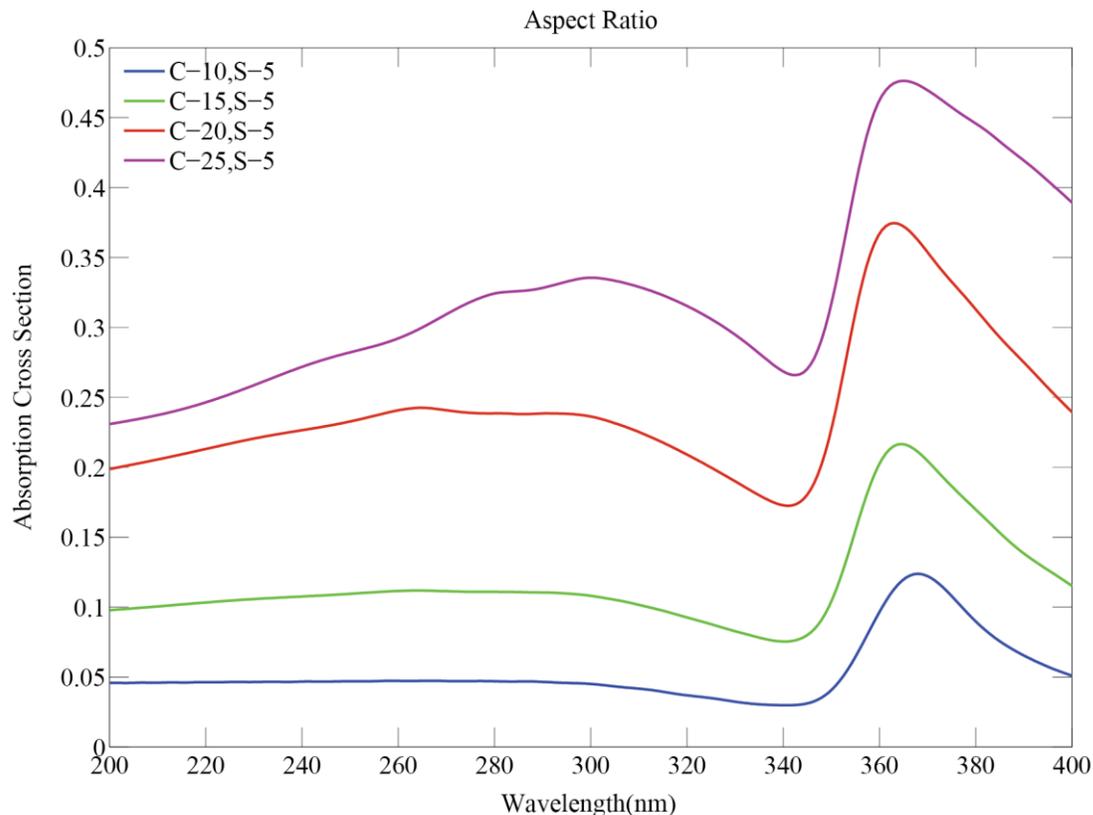
Figure 5.3 *Power Absorption curve of the Aspect Ratio*

The maximum point for each curve represents the First Order Values and the minimum points represent the Extraordinary values. The second maximum value represents the Higher Order Ordinary point for each curve. Upon increasing the core radius, the power absorption increases for all the points. Moreover, the wavelengths of all the points remain approximately the same.

For each of the extraordinary, ordinary and the First Order points, we have observed the electric field coupling. This is done to compare how the field coupling changes with respect to the core-shell ratio.
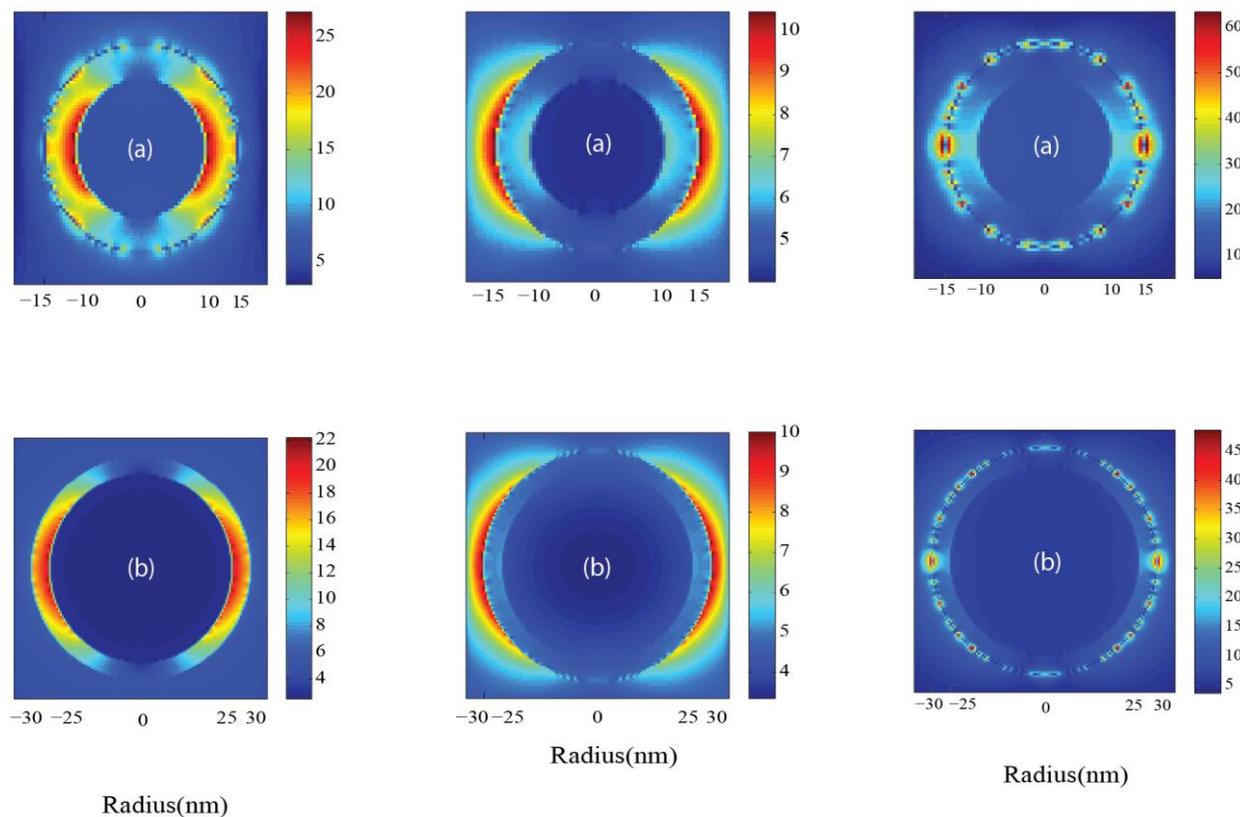
Figure 5.4 *Electric Field coupling diagram for Extraordinary, Ordinary and First Order Ordinary Plasmon Resonances respectively*

In the above figure, (a) represents C-10, S-5 and (b) represents C-25, S-5. For Extraordinary, it is seen that we have obtained quite effective coupling. It can also be deduced that the value of coupling decreases as we increase the radius of the core. Also the coupling is effective in (b). However, the change is not very significant (goes from a maximum value of around 27 to a maximum value of 22). For Ordinary, it is observed that the coupling is effective. While moving from (a) to (b), it is noticed that the maximum value of the coupling decreases slightly. We are ignoring the First Order because although the coupling is high, the electric field is scattered.

5.4 Sensitivity of Biomolecule

The objective of this part of the research is to understand how the sensitivity of the Extraordinary and the Ordinary points, and how the SPR shift vary with the change of its surrounding medium. This is obtained by using substances of different refractive indices. Here, water is used as the control medium and the variation is recorded with respect to water.

Sensitivity is calculated from the following formula:

$$Sensitivity = \frac{d\lambda}{dn}$$

Where, $d\lambda$ = Change in wavelength of incident light

dn = Change in refractive index

In this part, we are going to observe the characteristics for two fixed dimensions:
- Core: 25, Shell: 5
- Core: 20, Shell: 10

5.4.1 Core: 25, Shell: 5

For Extraordinary Mode:

The length of the shell and the radius of the core have been fixed at 5 nm and 25 nm respectively. Initially, the nanoparticle is immersed into water (refractive index: 1.33) and the corresponding P_{abs} curve is obtained. This curve gives us the point (wavelength of the incident light) at which the Extraordinary Resonance occurs. The simulation is repeated using different media such as Human Immunoglobulin G (IgG), Human Serum Albumin (HSA) and Lysozyme (Lys). This is done in order to change the refractive index of the surrounding media. The corresponding values of the wavelengths are recorded and a graph of Wavelength vs. Refractive Index is plotted. The slope of the curve gives us the value of Sensitivity.

The SPR shift due to the change in media can be calculated by taking the value of the wavelength obtained from water and subtracting it from the value of the wavelength of the next medium. A graph of SPR Shift vs. Surrounding Media is plotted. The results are tabulated below:

Table of Results:

Medium	Refractive Index, n	Wavelength/nm	SPR Shift/nm
H_2O	1.33	341.50	0.00
IgG	1.41	342.65	1.15
HAS	1.45	343.43	1.99
Lys	1.50	344.39	2.89

Graphical Representation of SPR Shift:
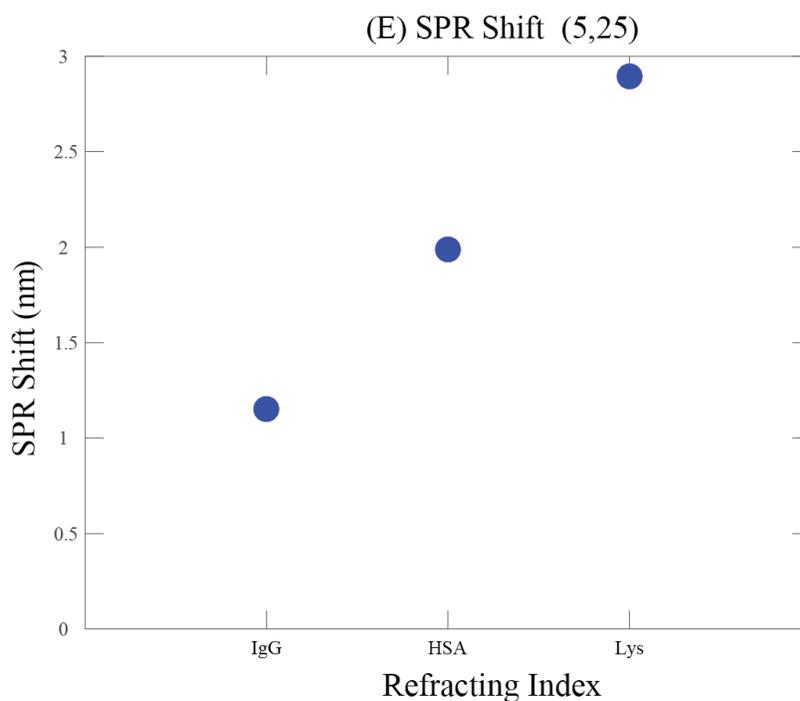
Figure 5.5 *SPR Shift for Extraordinary (C-25, S-5)*

After analyzing the graph, we can see the SPR Shift changing with respect to the change in refractive index. Therefore, we can assume a proportional relationship between the Refractive Index and the SPR Shift since there seems to be a linear relationship between the two variables.

Graphical Representation of Sensitivity:

Sensitivity of Extraordinary (5,25)
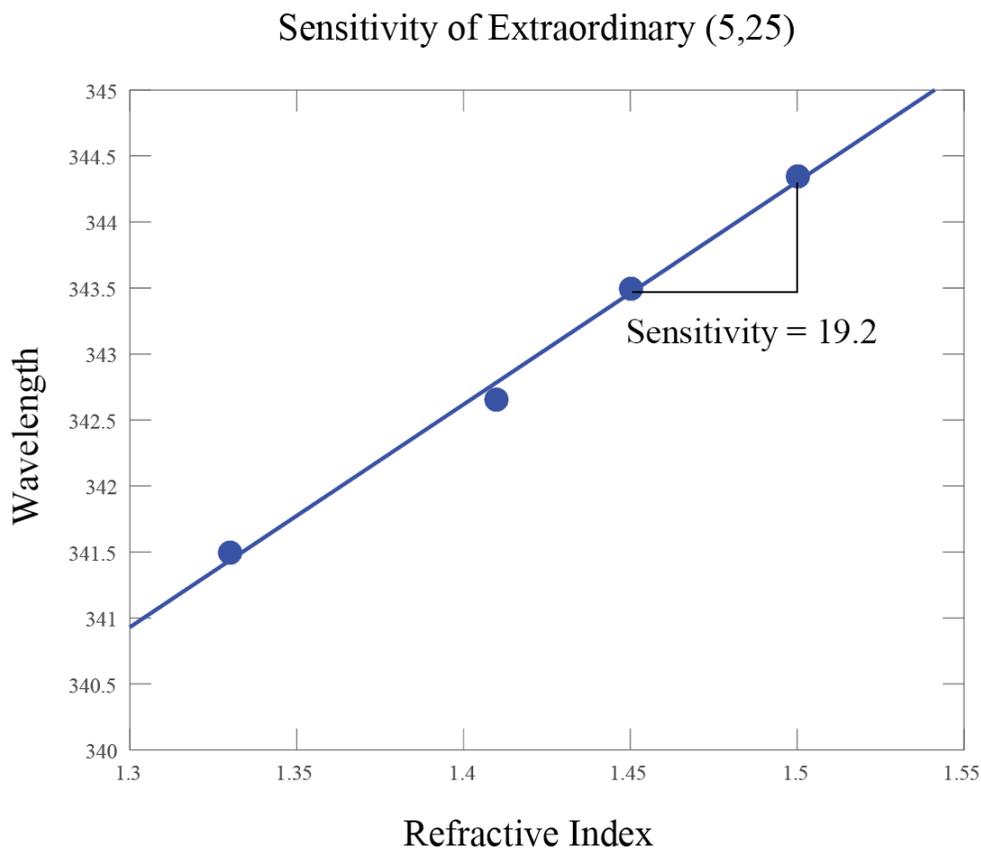
Figure 5.6 *Sensitivity of biomolecule for Ordinary (C-25, S-5)*

Calculation:

From the slope of the curve, the sensitivity is calculated:

$$Sensitivity = \frac{344.39 - 341.50}{1.50 - 1.33} = 19.2$$

For First Order Ordinary Mode:

We are observing the peak of the First Order Ordinary for the sensitivity because the SPR Shift is more visible compared to that of the Higher Order Ordinary peak. That is why we are considering only the First Order Ordinary for sensitivity.

Keeping everything the same as before, a new of set data are taken from the wavelength at which the First Order Ordinary resonance occurs. Two graphs are plotted again: SPR Shift vs. Refractive Index and Wavelength vs. Refractive Index. The table of results is given below:

Table of Results:

Medium	Refractive Index, n	Wavelength/nm	SPR Shift/nm
H_2O	1.33	359.459	0.000
IgG	1.41	362.086	2.627
HAS	1.45	363.727	4.268
Lys	1.50	365.215	5.756

Graphical Representation of SPR Shift:
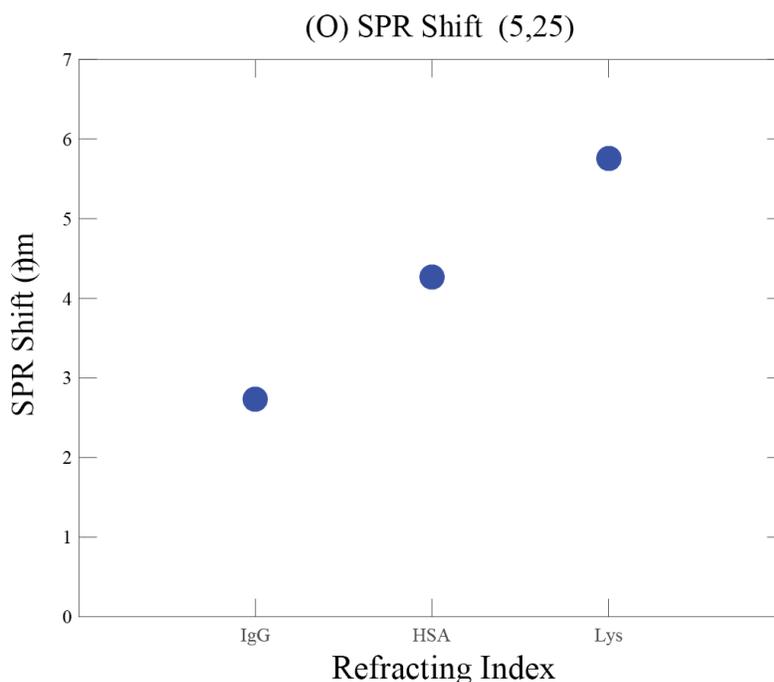
Figure 5.7 *SPR Shift for First Order Ordinary (C-25, S-5)*

After analyzing the graph, we can see the SPR Shift changing with respect to the change in refractive index. Therefore, we can assume a proportional relationship between the Refractive Index and the SPR Shift since there seems to be a linear relationship between the two variables.

Graphical Representation of Sensitivity:

Sensitivity of 1st Order Ordinary (5,25)

Sensitivity = 32.8

Figure 5.8 *Sensitivity of biomolecule for Ordinary (C-25, S-5)*

Calculation:

From the slope of the curve, the sensitivity is calculated:

$$Sensitivity = \frac{362.086 - 359.459}{1.41 - 1.33} = 32.8$$

5.4.2 Core: 20, Shell: 10

For Extraordinary Mode:

The length of the shell and the radius of the core have been fixed at 10 nm and 20 nm respectively. This is the only change that has been made for this section of our analysis. The same experiment is repeated by changing the refractive indices. A graph of Wavelength vs. Refractive index is plotted. The slope of the curve gives us the value of Sensitivity. Similarly, a graph of SPR Shift vs. Surrounding Media is plotted. The results are tabulated below:

Table of Results:

| Medium	Refractive Index, n	Wavelength/nm	SPR Shift/nm
H_2O	1.33	344.608	0.000
IgG	1.41	345.455	0.847
HAS	1.45	346.204	1.596
Lys	1.50	347.012	2.404

Graphical Representation of SPR Shift:

Figure 5.9 *SPR Shift for Extraordinary (C-20, S-10)*

After analyzing the graph, we can see the SPR Shift changing with respect to the change in refractive index. Therefore, we can assume a proportional relationship between the Refractive Index and the SPR Shift since there seems to be a linear relationship between the two variables.
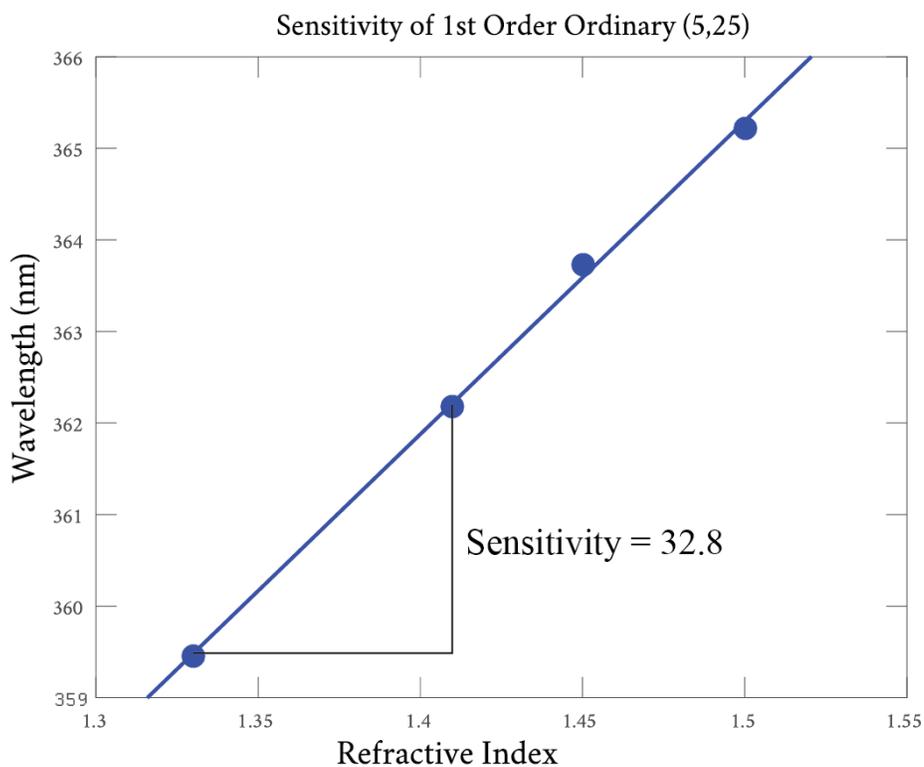
Graphical Representation of Sensitivity:
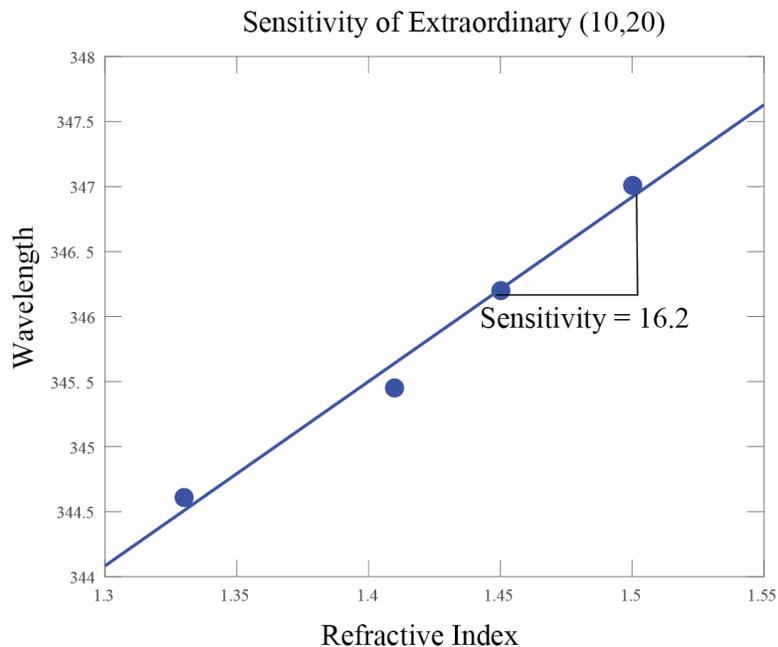
Figure 5.10 *Sensitivity of biomolecule for Ordinary (C-20, S-10)*

Calculation:

From the slope of the curve, the sensitivity is calculated:

$$Sensitivity = \frac{347.012 - 346.204}{1.5 - 1.45} = 16.2$$

For First Order Ordinary Mode:

Similar to what we have done before, we are observing the peak of the First Order Ordinary for the sensitivity because the SPR Shift is more visible compared to that of the Higher Order Ordinary peak. That is why we are considering only the First Order Ordinary for sensitivity.

Keeping everything the same as before, a new of set data are taken from the wavelength at which the First Order Ordinary resonance occurs. Two graphs are plotted again: Wavelength vs. Refractive Index and SPR Shift vs. Surrounding Media. The table of results is given below:

Table of Results:

Medium	Refractive Index, n	Wavelength/nm	SPR Shift/nm
H_2O	1.33	370.502	0.000
IgG	1.41	372.897	2.395
HAS	1.45	373.770	3.268
Lys	1.50	375.100	4.598

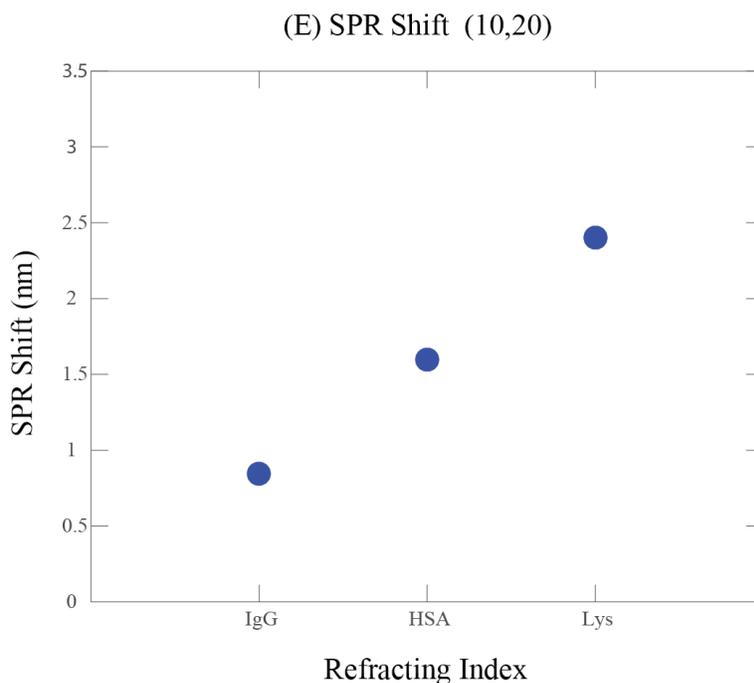**Graphical Representation of SPR Shift:**
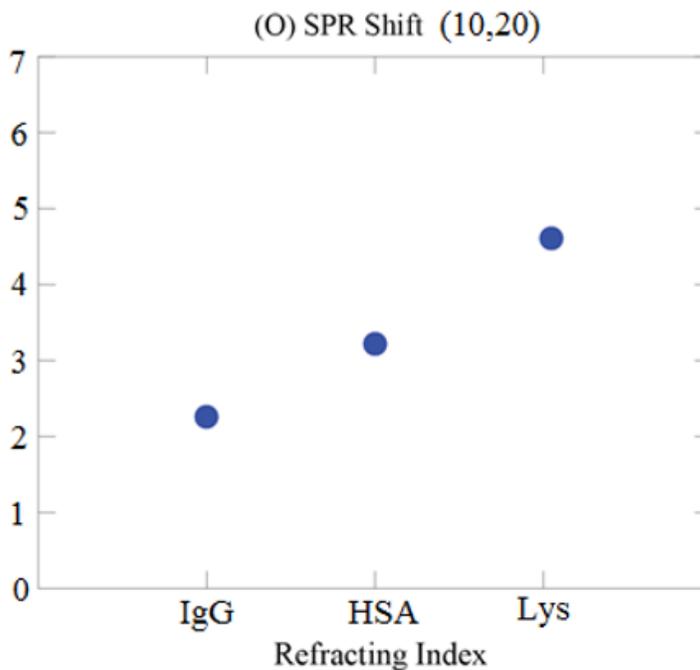
Figure 5.11 *SPR Shift for First Order Ordinary (C-20, S-10)*

After analyzing the graph, we can see the SPR Shift changing with respect to the change in refractive index. Therefore, we can assume a proportional relationship between the Refractive Index and the SPR Shift since there seems to be a linear relationship between the two variables.

Graphical Representation of Sensitivity:
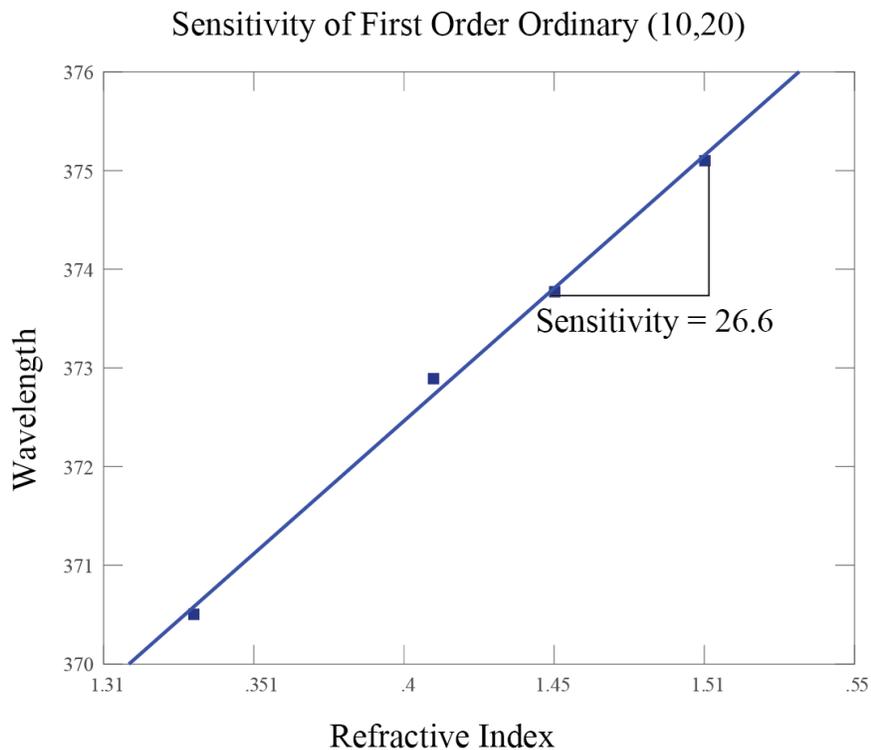
Figure 5.12 *Sensitivity of biomolecule for First Order Ordinary (C-20, S-10)*

Calculation:

From the slope of the curve, the sensitivity is calculated:

$$Sensitivity = \frac{375.100 - 373.770}{1.50 - 1.45} = 26.6$$

5.5 Substrate Effect

Titanium Dioxide (TiO_2) is a crystalline solid structure. It is used as an alternative to Silicon Dioxide (SiO_2) because it has very good stability, Hydrophilic properties, UV blocking ability and excellent photo catalytic abilities. TiO2 offers a range of physical and chemical properties that make it suitable for a wide spectrum of applications. We have compared the SPR shift that occurs due to the change in substrate and a corresponding graph of SPR Shift vs. Substrate is plotted.

The following analysis consists of a 20 nm radius core and 10 nm coated shell.

The refractive index of Titanium Dioxide is 2.61.
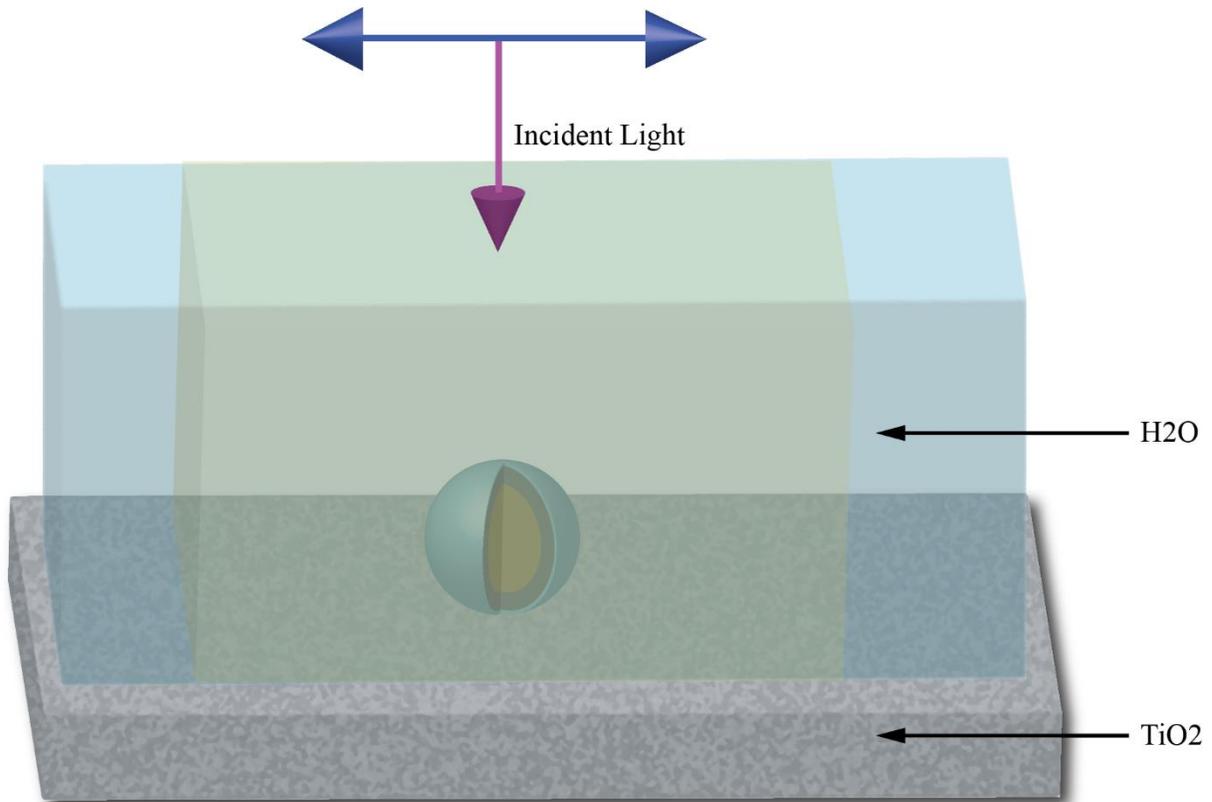
Figure 5.13 *Experimental setup with Titanium Oxide as the substrate*

For Extraordinary Mode:

The simulation is carried out with respect to the above assumptions and the corresponding results are tabulated below for extraordinary value of wavelength:

Table of Results:

Medium	Refractive Index	SiO$_2$		TiO$_2$	
		Wavelength (λ)	SPR Shift (dλ)	Wavelength (λ)	SPR Shift (dλ)
H$_2$O	1.33	344.608	0.000	345.455	0.000
IgG	1.41	345.455	0.847	346.204	0.749
HAS	1.45	346.204	1.596	346.755	1.345
Lys	1.50	347.012	2.404	347.712	2.257

Graphical Representation:

Figure 5.14 *SPR Shifts of SiO$_2$ and TiO$_2$ For Ordinary*

The SPR shift changes with regards to the change in substrate. From the above graph, we can come to the conclusion that the SPR Shift for TiO$_2$ is less compared to that of SiO$_2$.

For First Order Ordinary Mode:

The simulation is carried out with respect to the above assumptions and the corresponding results are tabulated below for First Order Ordinary value of wavelength:

Table of Results:

Medium	Refractive Index	SiO$_2$		TiO$_2$	
		Wavelength (λ)	SPR Shift (dλ)	Wavelength (λ)	SPR Shift (dλ)
H$_2$O	1.33	370.502	0.000	369.444	0.000
IgG	1.41	372.897	2.395	371.597	2.153
HAS	1.45	373.770	3.268	372.439	2.995
Lys	1.50	375.100	4.598	373.772	4.328

Graphical Representation:

Figure 5.15 *SPR Shifts of SiO$_2$ and TiO$_2$ for First Order Ordinary*
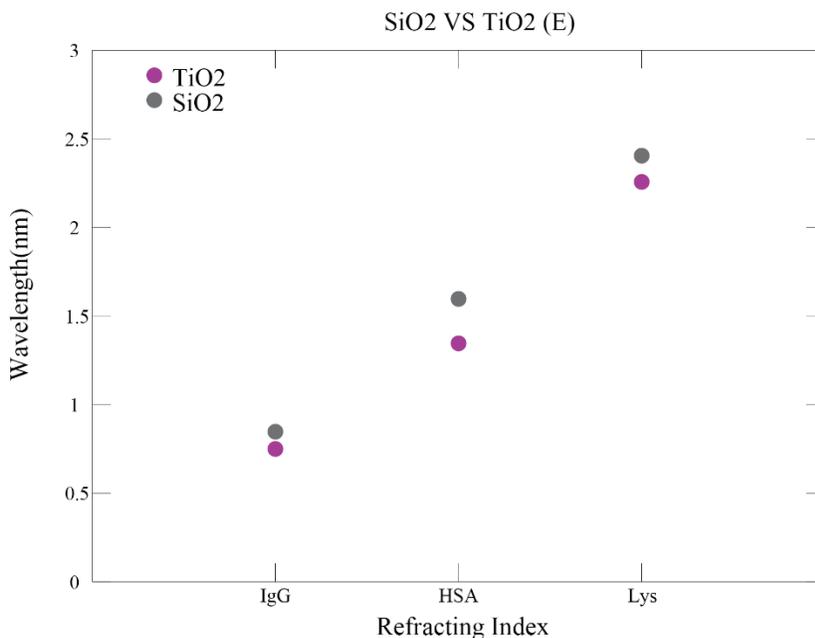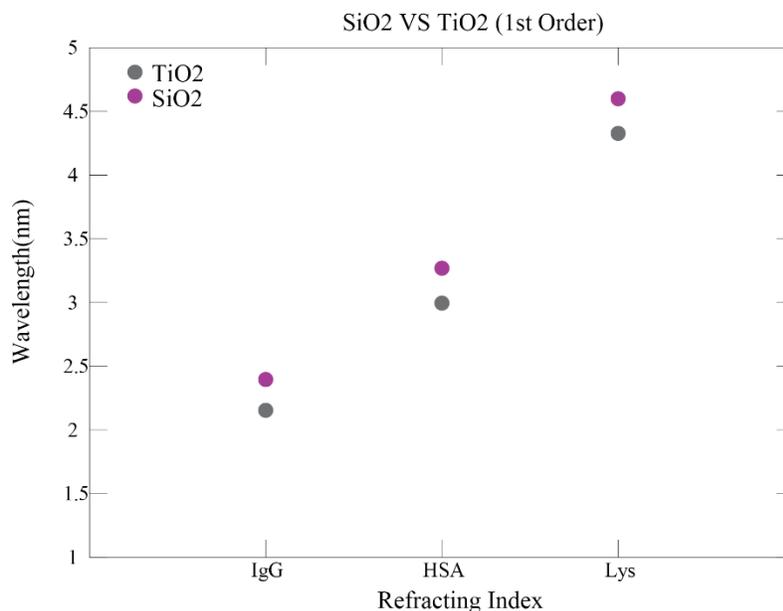
The SPR shift changes with regards to the change in substrate. From the above graph, we can come to the conclusion that the SPR Shift for SiO$_2$ is more compared to that of TiO$_2$ (similar to that of the Extraordinary mode). Moreover, the shift gap increases proportionally with the increase in refractive index.

6. Conclusion

This paper was done in the hopes of pursuing the unique characteristics of Localized Plasmon Resonance (LSPR) in colloidal nanoparticles. Besides its various applications in optics, photo catalysis, medicine and photovoltaics, we have seen its application in bio-sensing. The nanoparticle, comprised of a Gold core and a Silver shell, was placed on a substrate (preferably Silicon Dioxide). The setup was immersed in water and illuminated with light.

Our thesis research was based on the Extraordinary, Ordinary and First Order Ordinary Plasmon Resonances. The results and analysis was categorized into four sub-topics: Core-Shell Ratio, Aspect Ratio, Sensitivity of the biomolecule and the Substrate effect.

Core-Shell ratio analysis was carried out by changing the dimensions of the Gold core and the Silver shell of the nanoparticle. The substrate used for the analysis was Silicon Dioxide and the surrounding medium was water. Finally, the setup was illuminated with light. For these particular conditions, we have observed the Power Absorption curve and the Electric Field coupling, and have analyzed how they vary with respect to the change in magnitudes of the core and the shell.

Aspect ratio was carried out similarly; the substrate and the surrounding medium remained the same. The shell coating was fixed at a particular value and only the core radius was varied. Upon illumination and simulation, we obtain the Power Absorption curve and the Electric Field coupling. The pattern in which the variables change with regards to each other has been mentioned in the analysis and results.

Moreover, the sensitivity of the biomolecule was examined. For particular values of the core radius and the shell coating, and the same Silicon Dioxide substrate, the surrounding medium was being changed. Different media with different refractive indices were used in replacement with water and the analysis was done while keeping water as the control medium, i.e. all the data obtained were compared with the data that was obtained for water. We have observed the sensitivity of the biomolecule and the SPR Shifts due to the change in refractive indices.

Lastly, the replacement of Silicon Dioxide with Titanium Dioxide, whilst keeping the magnitude of the core and the shell fixed, gave us the Substrate Effect. The SPR Shift curves obtained from our research gave us a proper picture as to how the SPR Shift varies with respect to the change in refractive index.

One of the problems that we faced during our research was that we could not find the Extraordinary Resonance point initially. We had assumed that the Extraordinary Resonance value would be the second peak. However, that was not the case; the second peak value turned

out to be the point of Ordinary Resonance. The thought of the dark point being responsible for the Extraordinary Resonance value did not come to our minds because we had never thought that there could be Electric Filed coupling in a deep point, i.e. the minimum point. Therefore, we found the Extraordinary Resonance value at the dark point by intentionally choosing to work with it. We have come to see that the Extraordinary Resonance exists in values surrounding the dark point, but the Electric Field coupling is a maximum at the dark point.

Now the big question is: Why did we get an Extraordinary point in the dark value? One probable explanation might be, when we simulated monometallic Gold nanoparticle, the Power Absorption curve of Gold gave us a peak value at the same wavelength where we received a dark point in the bimetallic nanoparticle simulation. On the other hand, monometallic Silver nanoparticle gave us a high dark point in the same wavelength as the bimetallic nanoparticle simulation. As a result, there might be a possibility that the two phenomena of the individual metals intersected and gave an overall dark point.

Another explanation might be the generation of Fano Resonance. When two nanoparticles interact with each other, a Power Absorption curve is obtained, where there is a dark point. Researchers have changed the light source and observed that they obtain a tiny peak point where a Quadrupole was produced. That Quadrupole is known as Fano Resonance. We have predicted the generation of Fano Resonance in our paper upon observation because the Power Absorption of their research is almost similar to the Power Absorption curve that we have obtained.

References

[1] Zhang, C., Chen, B., Li, Z., Xia, Y., & Chen, Y. (2015). Surface Plasmon Resonance in Bimetallic Core-shell Nanoparticles. *The Journal of Physical Chemistry.* doi: 10.1021/acs.jpcc.5b04232

[2] Chin, C. W., (2011). Localized Surface Plasmon Resonance with the use of Silver and Titanium Oxide Nanostructures. p. 1. Retrieved from: http://web.utk.edu/~zzhang24/Chuck%20Chin%20Thesis.pdf

[3] Giannini, R. (1978). Shape Dependence of Localized Surface Plasmon Resonances and their application in nanoemmiters. Retrieved from: http://e-collection.library.ethz.ch/eserv/eth:47630/eth-47630-02.pdf

[4] Stockman, M. I., (2011). Nanoplasmonics: the physics behind the applications. *Physics Today*, 39-44. Retrieved from: http://physics.gsu.edu/stockman/data/Stockman_Phys_Today_2011_Physics_behind_Applications.pdf

[5] Maier, S. A. (2007) Localized Surface Plasmons. *Plasmonics: Fundamentals and applications*, p. 65-72. Retrieved from: https://www.london-nano.com/sites/default/files/uploads/research/highlights/Nanoplasmonics/pdf

[6] Plasmonics. Retrieved from: https://www.physik.hu-berlin.de/de.nano/lehre/Gastvorlesung%20Wien/plasmonics

[7] Surface Plasmon Resonance. Retrieved from: https://en.wikipedia.org/wiki/Surface_plasmon_resonance

[8] Raether, H. (1988). Surface Plasmons on Smooth and Rough Surfaces and on Gratings. *Springer Tractsin ModernPhysics*, Vol. 111, Springer Berlin

[9] Localized Surface Plasmon Resonance Theory. *Localized Surface Plasmon Resonance vs. Surface Plasmon Resonance*. Retrieved from: https://nicoyalife.com/technology/surface-plasmon-resonance/localized-surface-plasmon-resonance-theory/

[10] Free electron model (2016). Retrieved from: https://en.wikipedia.org/wiki/Free_electron_model

[11] Biomolecule (2016). Retrieved from: https://en.wikipedia.org/wiki/Biomolecule

[12] Lysozyme (2016). Retrieved from: https://en.wikipedia.org/wiki/Lysozyme

[13] Human Serum Albumin (2016). Retrieved from: https://en.wikipedia.org/wiki/Human_serum_albumin

[14] Immunoglobulin G (2016). Retrieved from: https://en.wikipedia.org/wiki/Immunoglobulin_G

[15] About Lumerical. *lumerical*. Retrieved from: https://www.lumerical.com/company/about_lumerical.html

[16] PDB-101: Lysozyme. Retrieved from:
https://www.google.com/search?q=lysozyme&client=firefox-b-ab&source=lnms&tbm=isch&sa=X&ved=0ahUKEwiy3oS81-rQAhUBVhQKHf5eBJoQ_AUICSgC&biw=1366&bih=657#imgrc=J0_6P2nRKcicaM%3A

[17] Immunoglobulin G. Causes, symptoms, treatment Immunoglobulin G. Retrieved from:
https://www.google.com/search?q=immunoglobulin+g&client=firefox-b-ab&source=lnms&tbm=isch&sa=X&ved=0ahUKEwia1KqJ2OrQAhVLthQKHca6D5cQ_AUICCgB&biw=1366&bih=657#imgrc=3CSnlav6ZTO0eM%3A

[18] Entertainment - Home Page. Retrieved from:
https://www.google.com/search?q=transmission+electron+microscope&client=firefox-b-ab&source=lnms&tbm=isch&sa=X&ved=0ahUKEwjq4sqK2erQAhVFXhQKHcpuBJUQ_AUICCgB&biw=1366&bih=657#tbm=isch&q=transmission+electron+microscope+images+of+nanoparticles&imgrc=GioadFCbmkDLhM%3A

[19] Scanning Electron Microscope. Retrieved from:
https://www.google.com/search?q=transmission+electron+microscope&client=firefox-b-ab&source=lnms&tbm=isch&sa=X&ved=0ahUKEwjq4sqK2erQAhVFXhQKHcpuBJUQ_AUICCgB&biw=1366&bih=657#tbm=isch&q=scanning+electron+microscope+images&imgrc=Ncm1bbJJJ40UYM%3A

[20] Lumerical Solutions, Inc. Retrieved from:
https://www.google.com/search?q=lumerical+solutions+logo&client=firefox-b-ab&source=lnms&tbm=isch&sa=X&ved=0ahUKEwjmxIj54-rQAhWFORoKHfhRBw4Q_AUICCgB&biw=1366&bih=657#imgrc=3iyJWdEBdavy3M%3A

[21] Symmetric and anti-symmetric BCs. Retrieved from:
https://kb.lumerical.com/en/index.html?ref_sim_obj_symmetric_anti-symmetric.html

[22] Periodic boundary conditions. Retrieved from:
https://kb.lumerical.com/en/index.html?ref_sim_obj_symmetric_anti-symmetric.html

[23] PML boundary conditions. Retrieved from:
https://kb.lumerical.com/en/index.html?ref_sim_obj_symmetric_anti-symmetric.html

[24] Mesh refinement. Retrieved from:
https://kb.lumerical.com/en/index.html?ref_sim_obj_symmetric_anti-symmetric.html

[25] Wilson, W. L., Szajowski, P. F. & Brus, L. E. (1993). Quantum confinement in size-selected surface-oxidized silicon nanocrystals. *Science* 262, 1242-1244.

[26] Durisic, N., Godin, A. G., Walters, D., Grutter, P., Wisemann, P. W. & Heyes, C. D. (2011). Probing the "dark" fraction of core-shell quantum dots by ensemble and single particle pH-dependent spectroscopy. *ACS Nano* 5, 9.62-9073.

[27] Verberk, R., Chon, J. W. M., Gu, M. & Orrit, M. (2005). Environment dependent blinking of single semiconductor nanocrystals and statistical aging of ensembles. *Physics E* 26, 19-23.

[28] Issac, A., Borczyskowski, C. & Cichos, F. (2005). Correlation between photoluminescence intermittency of CdSe quantum dots and self-trapped states in dielectric media. *Phys Rev. B* 71, 161302 (R).

[29] Bohren, C. F. & Huffman, D. R. (2004). Absorption and scattering of light by small particles. Wiley, Weinheim

[30] Prodan, E., Radloff, C., Halas, N. J. & Norlander, P. (2003). A hybridization model for the plasmon resonance of complex nanostructures. *Science* 302, 419-422.

[31] Klar, T. A. & Feldmann, J. (2012). Complex-shaped metal nanoparticles: Bottom-up syntheses and applications. Edited by Sau, T. K. & Rogach, A. L. Viley, chapter 12

[32] Lakowicz, J. R. (2005). Radiative decay engineering 5: Metal-enhanced fluorescence and plasmon emission. *Anal. Biochem.* 337, 171-194.

[33] Anker, J. N., Hall, W. P., Lyandres, O., Shah, N. C., Zhao, J. & Van Duyne, R. P. (2008). Biosensing with plasmonic nanosensors. *Nature Materials* 7, 442-453.

[34] Malinsky, M. D., Kelly, K. L., Schatz, G. C. & Van Duyne, R. P. (2001). Chain length dependence and sensing capabilities of the localized surface plasmon resonance of silver nanoparticles chemically modified with alkanethiol self-assembled monolayers. *J. Am. Chem. Soc.*123, 1471-1482.

[35] Willets, K. A. & Van Duyne, R. P. (2007). Localized Surface Plasmon Resonance Spectroscopy and Sensing. *Annu Rev. Phys. Chem.* 58, 267-297.

[36] Khalavka, Y. Becker, J. & Sönnichsen, C. (2009). Synthesis of rod-shaped gold nanorattles with improved plasmon sensitivity and catalytic activity. *JACS* 131, 1871-1875.

[37] Kravets, V. G., Schedin, F., Kabashin, A. V. & Grigorenko, A. N. (2009). Sensitivity of collective plasmon modes of gold nanoresonators to local environment. *Opt. Lett.* 35, 956-958.

[38] Pillai, S., Catchpole, K. R., Trupke, T. & Green, M. A. (2007). Surface plasmon enhanced silicon solar cells. *J. Appl. Phys.* 101, 093105.

[39] Smith, D. R., Pendry, J. B. & Wiltshire, M. C. K. (2004). Matamaterials and negative refractive index. *Science.* 305, 788-792.

[40] Li, D., Qin, L., Qi, D. X., Gao, F., Peng, R. W., Zou, J., Wang, Q. J. & Wang, M. (2010). Tunable electric and magnetic resonances in multilayered metal/dielectric nanoplates at optical frequencies. *J. Phys. D: Appl. Phys.* 34,345102.

[41] Barnes, W. L. (2006). Surface plasomn-polariton length scales: A route to sub-wavelength optics. *J. Opt. A: Pure Appl. Opt.* 8, S87-S93

[42] Maier, S. A., Kik, P.G. Atwater, H. A., Meltzer, S. Harel, E. Koel, B. E. & Requicha, A. A. A. G. (2003). Local detection of electromagnetic energy transport below the diffraction limit in metal nanoparticle plasmon waveguides. *Nature* 2, 229-232.

[43] Ozbay, E. (2006). Merging photonics and electronics at nanoscale dimensions. *Science* 311, 189-193.

[44] Walters, R. J., van Loon, R. V. A., Brunets, I., Schmitz, J. & Polman, A. (2010). A silicon-based electrical source of surface plasmon polaritons. *Nature Materials* 9, 21-25.

[45] Ringe, E., Langille, M. R., Sohn, K., Zhang, J., Mirkin, C. A., van Duyne, R. P. & Marks, L. D. (2012). Plasmon length: A universal parameter to describe size effects in gold nanoparticles.

[46] Ringe, E., Zhang, J., Langille, M. R., Mirkin, C. A., Marks, L. D., van Duyne, R. P. (2012). Correlating the structure and localized surface plasmon resonance of single silver right bipyramids. *Nanotech* 23, 444005.

[47] Myroshnychenko, V., Rodriguez-Fernandez, J. R., Pastoriza-Santos, I., Funston, A.M., Novo, C., Mulvaney, P., Liz-Marzan, L. M. & Garcia de Abajo, F. J. (2008). Modelling the response of gold nanoparticles. *Chem. Soc. Ref.* 37, 1792.

[48] Temple, T. L. & Bagnall, D. M. (2011). Optical properties of gold and aluminium nanoparticles for silicon solar cell applications. *J. Appl. Phys.* 109, 084343.

[49] Knight, M. W., Wu, Y., Lassiter, J. B. & Halas, N. J. (2009). Substrate matter: Influence of an adjacent dielectric on an individual plasmonic nanoparticle. *Nano Lett.* 9, 2188-2192.

[50] Vernon, K. C., Funston, A. M., Novo, C., Gomez, D. E., Mulvaney, P. & Davis, T. J. (2010). Influence of particle-substrate interaction on localized plasmon resonances. *Nano Lett.* 10, 2080-2086.

[51] Noguez, C. (2007). Surface plasmons on metal nanoparticles: the influence of shape and physical environment. *J. Phys. Chem.* C 111, 3806-3819.

[52] Kelly, K. L., Coronado, E., Zhao, L. L. & Schatz, G. C. (2003). The optical properties of nanoparticles: The influence of size, shape, and dielectric environment. *J. Phys. Chem.* B 107, 668-677.

[53] Ming, T., Zhao, L., Yang, Z., Chen, H., Sun, L., Wang, J. & Yan, C. (2009). Strong polarization dependence of plasmon-enhanced fluorescence on single gold nanorods. *Nano Lett.* 9, 3896-3903.

[54] Thompson, P. G., Biris, C. G., Osley, E. J., Gaathon, O., Osgood Jr., R. M., Panoiu, N. C. & Warburton, P. A. (2011). Polarization-induced tunability of localized surface plasmon resonances in arrays of sub-wavelength cruciform apertures. *Opt. Express* 19, 25035-25047.

[55] Kooij, E. S. & Poelsema, B. (2006). Shape and size effects in the optical properties of metallic nanorods. *Phys, Chem. Chem. Phys.* 8, 3349-3357.

[56] Kooij, E. S., Ahmed, W., Zandvliet, H. J. W. & Poelsema, B. (2011). Localized surface plasmons in noble metal nanospheroids. *J. Phys. Chem. C* 115, 10321-10332.

[57] Sönnichsen, C., Franzi, T., Wilk, T., von Plessen, G & Feldmann, J. (2002). Drastic reduction of plasmon damping in gold nanorods. *Phys, Rev. Lett.* 88, 077402.

[58] Zoric, I., Zach, M., Kasemo, B., & Langhammer, C. (2011). Material independence, subradiance, and damping mechanisms. *ACS Nano* 5, 2535-2546.

[59] Sönnichsen, C., Franzl, T., von Plessen, G. & Feldmann, J. (2002). Plasmon resonances in large noble-metals clusters. *New Journal of Physics* 4, 93. 1-93.8.

[60] (2000). Light scattering by nonspherical particles. Edited by Mishchenko, M. I., Hovenier, J. W. & Travis, L. D., Academic Press.

[61] Novotny, L. & Brecht, B. (2006). Principles of nano-optics. University Press, Cambridge.

[62] Hohenester, U. & Krenn, J., (2005). Surface plasmon resonances of single and coupled metallic nanoparticles: A boundary integral method approach. *Phys. Rev. B* 72, 195429.

[63] Berkovitch, N., Ginzburg, P. & Orenstein, M. (2012). Nano-plasmonic antennas in the near infrared regime. *J. Phys.: Condens. Matter* 24, 073202.

[64] Mock, J. J., Barbic, M., Smith, D. R., Schultz, D. A. & Schultz, S. (2002). Shape effects in plasmon resonance of individual colloidal silver nanoparticles. *J. Chem. Phys.* 116, 6755-6759

[65] Bryant, G. W. (2008). Mapping the plasmon resonances of metallic nanoantennas. *Nano Lett.* 8, 631-363.